Determinants of amyloid fibril degradation by the PDZ protease HTRA1

Simon Poepsel[1], Andreas Sprengel[1], Barbara Sacca[1], Farnusch Kaschani[1], Markus Kaiser[1], Christos Gatsogiannis[2], Stefan Raunser[2], Tim Clausen[3] and Michael Ehrmann[1,4] *

[1] *Centre of Medical Biotechnology, Faculty of Biology, University Duisburg-Essen, Universitaetsstrasse, 45141 Essen, Germany*

[2] *Department of Structural Biochemistry, Max Planck Institute Molecular Physiology Otto Hahn Str. 11, 44227 Dortmund, Germany*

[3] *Research Institute of Molecular Pathology – IMP, Dr. Bohrgasse 7, 1030 Vienna, Austria*

[4] *School of Biosciences, Cardiff University, Cardiff CF10 3US, UK*

[*] **Corresponding author:**

Email: michael.ehrmann@uni-due.de, Phone: +49-201-183 2949

Running title: Proteolysis of amyloid fibrils by HTRA1

ABSTRACT

Excessive aggregation of proteins has a major impact on cell fate and is a hallmark of amyloid diseases in humans. To resolve insoluble deposits and to maintain protein homeostasis, all cells employ dedicated protein disaggregation, protein folding and protein degradation factors. Despite intense recent research, the underlying mechanisms controlling this key metabolic event are not well understood. Here, we have analyzed how a single factor, the highly conserved serine protease HTRA1, degrades amyloid fibrils in an ATP-independent manner. This PDZ-protease solubilizes protein fibrils and disintegrates the fibrillar core structure allowing productive interaction of aggregated polypeptides with the active site for rapid degradation. Thereby, aggregate burden in a cellular model of cytoplasmic tau aggregation is reduced. Mechanistic aspects of ATP-independent proteolysis and its implications in amyloid diseases are discussed.

INTRODUCTION

Misfolded polypeptides or protein fragments can associate into insoluble protein aggregates, e.g. inclusion bodies and amyloid fibrils. Inclusion bodies are commonly observed when overproducing recombinant proteins and are characterized by an amorphous surface[1]. Amyloids arising from native proteins or protein fragments comprise fibrils formed by ordered β-sheets that can also form helical filaments and are hallmarks of degenerative protein folding diseases[2].

To counteract the potential lethal effects of misfolded proteins and insoluble aggregates, protein quality control systems perform protein diagnosis, repair and degradation. Individual misfolded proteins are considered easier targets of protein

quality control compared to insoluble aggregates because the accessibility of the individual constituents of tightly packed amyloids is limited. Therefore, recent research has addressed the important question of protein disaggregation as a prerequisite of efficient protein repair and degradation. The most widely studied factors involved in protein disaggregation belong to the classic heat shock protein (Hsp) family[3], members of which are chaperones and co-chaperones of the Hsp40, 70, 90 and Hsp104 subclasses. Current data suggest a concerted cooperation of the Hsp40, 70 and Hsp104 (AAA^+) chaperones in protein disaggregation with the final, ATP-fuelled threading of individual, unfolded substrate proteins through the central pore of Hsp104 being essential for disrupting the tight aggregate structure. Subsequently, these unfolded polypeptides are released for either refolding or proteolytic degradation (for review, see[4]). However, a single protein that is able to eliminate fibrillar aggregates and harbors both dissolving and proteolytic functions is unknown.

Human HTRA1 belongs to the widely conserved family of high-temperature requirement A (HtrA) proteins that function as ATP-independent serine proteases in protein quality control and stress response pathways[5,6]. Individual HtrAs mediate sensing, repair and degradation of damaged, fragmented and mislocalized proteins. Defining features of HtrA proteases are their homooligomeric architecture and C-terminal PDZ domains that preferentially bind to surface exposed tri- or tetrapeptide motifs. PDZ domains of HtrA proteases can be involved in sensing of misfolded proteins, substrate processing, allosteric and cooperative regulation of the proteolytic activity and in the switch between various oligomeric states (for review, see[6]).

Ubiquitously expressed human HTRA1 consists of a signal sequence for secretion, a partial insulin like growth factor binding protein-7 (IGFBP-7) domain, a serine

protease domain and one C-terminal PDZ domain. Like all other HtrAs, HTRA1 switches reversibly between active and inactive conformations. While the PDZ domain of HTRA1 has not been implicated in allosteric regulation, it contributes to substrate processing, as a PDZ deletion affects the length of cleavage products[7]. In addition, the PDZ domain binds specific interaction partners, which seems one way of regulating the subcellular location of HTRA1[8].

HTRA1 is found in three subcellular locations. Secreted HTRA1 is involved in the homeostasis of the extracellular matrix[9-14] and intracellular HTRA1 was localized to the cytoplasm, to microtubules and to the nucleus[8,15,16]. Microtubule-associated HTRA1 degrades tubulins, thereby inhibiting cell migration[8,17]. Moreover, HTRA1 has been implicated in several severe pathologies including cancer, age-related macular degeneration, Alzheimer's disease (AD), arthritis and familial ischemic cerebral small-vessel disease[10-12,18-22]. In these diseases, protein fragments or aggregates are either causative for disease or are disease modifying factors that are produced or degraded by HTRA1.

The microtubule-associated protein tau aggregates into intracellular neurofibrillary tangles representing one hallmark of AD and other tauopathies. Normal tau is thought to regulate microtubule dynamics. Interaction of tau with microtubules is mediated by its microtubule binding domain (MTBD) composed of several pseudorepeats sharing the consensus sequence VxSKxGSxxN(L/I)xHxPGGG. Typically resulting from an abnormally high degree of phosphorylation, free tau protein mislocalizes to the somatodendritic compartment of neurons, where it polymerizes into straight or paired helical filaments (PHF), ribbons and other conformations. The core domain of PHFs consists of three or four repeats of MTBD mediating tau-tau interactions. In addition, proteolytic processing by e.g. caspases[23] or lysosomal proteases[24] of tau may drive

fibril assembly. The progressive growth of such aggregates by capturing further tau proteins contributes to cell death and therefore pathological features (for review see[25]).

Recent studies suggest that several HtrAs act as protein quality control proteases that digest un- or misfolded proteins but not folded proteins (for review see[6]). In addition, HTRA1 degrades aggregated and fibrillar tau[26]. As substrate cleavage requires the precise positioning of an isolated peptide stretch to the proteolytic site, the local disruption of tight fibrillar interactions should be a prerequisite for efficient degradation. Here, we show that HTRA1 uses fibril disintegration as an integral aspect of its proteolytic activity towards amyloid fibrils and thus combines disintegration and protease activities in a single protein. Strikingly, the intrinsic disintegration activity of HTRA1 facilitates proteolysis of tau fibrils thereby reducing the aggregate burden in a cellular model of cytoplasmic tau aggregation.

RESULTS

HTRA1 disintegrates tau fibrils

As HTRA1 digests tau fibrils[26], we sought to identify a potential disintegration activity of HTRA1 that would improve proteolytic degradation of inaccessible substrates. To assay disintegration separately from proteolysis, we used the proteolytically inactive variant HTRA1 Ser328Ala for initial experiments. Fibrils of the 441 residue isoform (4R) of tau[26,27] were incubated with or without equimolar amounts of HTRA1 S328A or the control protein aldolase. Disintegration, the product of which is soluble tau, was analyzed by sedimentation assays using ultracentrifugation. While incubation of fibrils with HTRA1 S328A yielded mainly soluble tau, incubation with aldolase had insignificant effects on the relative amount

of soluble tau (Fig. 1a, left panel and Supplementary Results, Supplementary Fig. 1a). Note that HTRA1 S328A and aldolase were almost completely soluble under the conditions tested (Fig. 1a, right panel). Moreover, a titration experiment revealed a dose-dependent effect on the solubilization of tau fibrils by HTRA1 S328A (Supplementary Fig. 1b).

To investigate whether fibrils composed of the MTBD of tau are also solubilized, we repeated the sedimentation assays using a 3 fold molar excess of HTRA1 S328A. Note that these fibrils are packed more tightly compared to 4R tau fibrils[28] and exhibit SDS-resistant tau dimers in SDS-PAGE (Supplementary Fig. 1c, top panel). Again, incubation of these fibrils with HTRA1 S328A led to soluble tau, while incubation with the control aldolase was ineffective (Supplementary Figures 1c, top panel and 1d). In the absence of MTBD tau, HTRA1 and aldolase were in the soluble fraction, while HTRA1 S328A was both in the soluble and pellet fractions upon incubation with MTBD aggregates (Supplementary Fig. 1c, bottom panels). The reason for insoluble HTRA1 is unknown. Presumably, HTRA1 binds tightly to residual fibrils resistant to disintegration and is therefore co-sedimented during ultracentrifugation (Supplementary Fig. 1c, bottom left).

Quantification via atomic force microscopy (AFM)

To obtain independent and quantitative experimental evidence, disintegration was assessed by a single molecule approach. AFM of untreated samples revealed individual fibrillar structures of various lengths (0.1 up to >2 μm) and a characteristic width of around 20 – 25 nm as described[26,29]. AFM analyses were performed after incubation with or without equimolar amounts of HTRA1 S328A (Fig. 1b) or the isolated PDZ domain of HTRA1 as a control (Fig. 1c). For quantification of fibril

abundance in each sample, the lengths of individual fibrils were measured and added up to obtain a value of total fibril length. Comparison of these data indicated that incubation with HTRA1 S328A caused a statistically significant, 4 fold reduction of the amount of fibrils, whereas incubation with the PDZ domain alone did not (Supplementary Fig. 2a,b). Also, assessment of the distribution of fibril size revealed that disintegration was independent of their length (Supplementary Fig. 2c), indicating that no subset of fibrils was preferentially disintegrated or resistant to disintegration.

Internalization of recombinant HTRA1 by cultured cells

Subsequently, we examined whether disintegration of fibrils occurs in living cells. We established cellular tau aggregation and an alternative approach of introducing defined amounts of HTRA1 into human cells, i.e. uptake of purified recombinant protein from the cell culture medium without protein transfection reagents (Supplementary Fig. 3a,b). This method excludes problems arising from plasmid transfection i.e. heterogeneity and uncontrolled protein levels within a batch of cells. Importantly, confocal microscopy revealed colocalization of internalized HTRA1 S328A with both its native cytosolic substrate tau and endogenous HTRA1 (Supplementary Fig. 3c,d). The secondary antibody control did not show any signal with the respective settings (Supplementary Fig. 3e).

Disintegration of intracellular tau fibrils

Aggregation of cytoplasmic tau in 293T HEK cells (transiently overexpressing HA-tagged tau) was induced by seeding with fragmented MTBD fibrils[30]. Staining of cells with the amyloid specific fluorescent dye Thioflavin S (ThS) and immunostaining of

tau show that cells were loaded with aggregated tau (Fig. 2a). In addition, distinct colocalization of HTRA1 and tau fibrils was observed in cells treated with recombinant HTRA1 S328A (Fig. 2b, arrowheads).

Subsequently, we tested the effect of HTRA1 S328A on aggregated tau levels (Fig. 2c). Cells containing tau fibrils were treated with recombinant HTRA1 S328A and incubated for 20 h, followed by sarkosyl extraction of cell lysates. Pellet fractions from this extraction contain tau aggregates whereas supernatants contain soluble tau. These fractions were subjected to Western blotting using antibodies against tau and HTRA1. Quantification of band intensities revealed a significant and about 3 fold lower amount in sarkosyl insoluble tau in HTRA1 S328A treated cells compared to the PBS control (Fig 2c, middle panel and Supplementary Fig. 4a), while there were no marked differences in soluble tau levels (Fig. 2c, left panel).

Disintegration enhances proteolysis of tau fibrils

Fibril disintegration by HTRA1 should improve the accessibility of individual tau polypeptides to the active site, thus allowing enhanced proteolysis. To test this model, we established experimental conditions to measure the effects of disintegration on proteolytic digestion. This approach combines pre-treatment of fibrils with HTRA1 S328A before adding low amounts of proteolytically active HTRA1. Therefore, purified tau fibrils were preincubated with HTRA1 S328A for 2 h and subsequently incubated with proteolytically active HTRA1 (Fig. 3a, right panel). Indeed, fibrillar tau was more efficiently digested following preincubation with HTRA1 S328A compared to preincubation with buffer or PDZ domain controls (Fig. 3a, left and lower panel, respectively). Moreover, HTRA1's disintegration activity should not lead to improved processing of soluble tau because it is an unstructured substrate[31]. As

expected, soluble tau was not digested more rapidly following preincubation with HTRA1 S328A (Fig. 3b). In contrast, the presence of HTRA1 S328A led to slightly slower digestion of soluble tau, probably because of competitive binding to tau.

To obtain additional evidence for the model that disintegration activity acts mainly on fibrils, we incubated fibrillar and soluble tau with a 10 fold higher concentration of proteolytically active HTRA1 (Supplementary Fig 5a). At these increased levels, active HTRA1 is able to efficiently perform both disintegration and proteolysis. Clearly, higher protease concentrations strongly improved the digestion of fibrils (compare left panels of Fig. 3a and Supplementary Fig. 5a) but not of soluble tau (compare left panel of Fig. 3b and right panel of Supplementary Fig. 5a).

Using the cellular model of tau aggregation (Fig. 2), we asked whether added proteolytically active HTRA1 would reduce the levels of aggregated tau. Cells containing seeded tau aggregates were treated with recombinant HTRA1 or PBS for 20 h. Subsequently, sarkosyl extraction of cell lysates yielded pellet fractions containing aggregates and supernatants containing soluble tau. As expected, cells treated with HTRA1 had ca. 6 fold less tau aggregates as compared to the PBS controls (Supplementary Fig. 4b, top and bottom right panels). While the levels of soluble tau were reduced in HTRA1 treated cells that were not seeded with fibril fragments, in agreement with previously published data[26], there were no marked differences of soluble tau levels in cells treated with seeds (Supplementary Fig. 4b, left panel). The latter might be explained by a preference of HTRA1 for fibrils compared to soluble tau, as suggested above.

Quantification of proteolysis following disintegration

To quantify improved proteolytic processing of tau fibrils, the protease assays described (Fig. 3a,b) were repeated and samples were analyzed by AFM. Fibrillar tau was either preincubated with HTRA1 S328A or controls (buffer or PDZ domain of HTRA1) for 2 h, followed by incubation with active HTRA1 (Fig. 3c, Supplementary Fig. 5b). Quantification of fibril degradation was done as before (Supplementary Fig. 2a,b). Digestion with HTRA1 alone or digestion following incubation with HTRA1's PDZ domain caused an about 2 fold reduction of fibrils. Notably, preincubation with HTRA1 S328A followed by incubation with active HTRA1 caused a statistically highly significant, 6 fold reduction in the amount of fibrils (Fig. 3c). Moreover, assessment of the distribution of fibril size revealed that disintegration occurred independently of their length (Supplementary Fig. 5c) corresponding to the analyses after disintegration only (Supplementary Fig. 2c).

Mechanism of degradation of tau fibrils

Single molecule analyses of fibrils were performed to further explore the mechanism of proteolysis. Fibril disintegration and proteolysis could either be a directional process initiated at the free ends of fibrils or involve the action of HTRA1 along the whole fibril length. To directly visualize the binding of HTRA1 to fibrils, negative-stain electron microscopy (EM) was employed. Fibrils incubated with equimolar amounts HTRA1 S328A prior to their isolation and negative staining clearly showed a regular decoration along each fibril (Fig. 4a, (B)) while buffer treated fibrils did not (Fig. 4a, (A)). This decoration was even more pronounced when increasing the ratio of HTRA1:tau (Fig. 4a, (C)), although under these conditions HTRA1 seemed to occasionally dissociate from the fibrils, as seen from the sporadic single particles in

the background. Notably, the fibrils decorated with HTRA1 had a larger diameter than those without bound HTRA1 (Fig. 4a, inlets).

Total internal reflection fluorescence microscopy (TIRFM) allowed us to directly observe the degradation of fluorescently labeled tau fibrils during incubation with active HTRA1 in real time (Fig. 4b,c, Supplementary Fig. 6). In accordance with the EM data (Fig. 4a), the fluorescence decreased across the entire length of the fibrils, rather than starting from the fibril ends, suggesting that proteolysis is not directional. This conclusion was supported by determining the relative decrease of fluorescence along the fibrils (Supplementary Fig. 6a).

Quantification of fibril degradation during 10 h incubation showed a 68% decrease in fluorescence in the presence of HTRA1 compared to 29% in the buffer control, the latter being the result of bleaching (Supplementary Fig. 6b). Also, images of single endpoints, i.e. in the absence of repeated exposures and thus photobleaching, revealed decreased fluorescence of fibrils compared to buffer control (Supplementary Fig. 6c). Similar data were obtained at high temporal resolution during 4 h incubation even though the buffer control showed considerable effects of bleaching (Supplementary Video 1 and 2). HTRA1 degrades labeled fibrils as assessed by SDS-PAGE underlining that TIRFM data reflect degradation rather than removal of label (data not shown).

To obtain further insights into how the intrinsic disintegration activity of HTRA1 contributes to proteolysis, the occurrence of proteolytic products was followed over time. Fibrils were preincubated with HTRA1 S328A and subsequently incubated with active HTRA1 for various times or preincubated with buffer as a control (Fig. 5, green and orange bars, respectively). Peptidic products identified by mass spectrometry were mapped to sections of the primary amino acid sequence of tau.

After 3 h digestion, fibrils preincubated with or without HTRA1 S328A had 10 cuts in the tightly packed core region and 16 cuts in non-core regions versus no cuts in core and 3 cuts in non-core regions, respectively (Fig. 5a left panel). Even after overnight digestion without preincubation, HTRA1 performed only 2 cuts within the core region (Fig. 5a right panel). Overall in the o/n samples, proteolytic processing lead to a total of 34 vs. 10 cuts with and without preincubation, respectively (Fig. 5a right panel). Differences in digestion of soluble tau were less pronounced as soluble tau was also cleaved within the core region without preincubation with HTRA1 S328A, as expected (Fig. 5b).

The mass spectrometry data indicate that, without preincubation with HTRA1 S328A, HTRA1 initiates processing of fibrils from the less tightly packed N- and C-termini, of tau proceeding into the core regions only at later time points, probably once the core regions were destabilized by disintegration or the initial cuts. Critically, the disintegration activity of HTRA1 significantly enhances the immediate proteolytic processing of tightly packed regions of fibrils leading to an overall more efficient degradation.

To obtain further direct and independent experimental evidence of binding of specific tau sequences to HTRA1, peptides were synthesized corresponding to various regions of tau. The dissociation constants (K_D) for binding to HTRA1 were measured by isothermal titration calorimetry (ITC) (Supplementary Fig. 7). Peptides corresponding to residues 298-309 in the repeat region exhibited a K_D of 25 μM, while peptides corresponding to residues 385-393 or 385-399 had K_Ds of 35 μM and 40 μM, respectively. Peptides corresponding to residues 247-256 and 402-417 did not bind to HTRA1. These data reveal sequence specificity of the interaction of tau with HTRA1 and thus of disintegration and proteolysis.

Role of HTRA1's PDZ domain in fibril disintegration

Binding of peptides to the PDZ domains of HtrA proteases has been implicated in substrate binding, allosteric regulation and subcellular location. Therefore, we reasoned that the PDZ domain might contribute to fibril disintegration. To test this assumption, an HTRA1 S328A ΔPDZ construct was purified and its ability to disintegrate fibrils was assessed by sedimentation, AFM, preincubation in combination with subsequent protease assays, mass-spectrometric analysis of cleavage products, and in cell-based assays of tau aggregation (Fig. 6a-e).

Neither HTRA1 S328A ΔPDZ, nor the isolated PDZ domain was able to solubilize fibrils composed of full-length tau (Fig. 6a, Supplementary Fig. 8a) or MTBD tau (Supplementary Fig. 8c,d) in sedimentation assays and AFM analyses (Fig. 6b, 1c, Supplementary Fig. 8b). While HTRA1 S328A remained in the supernatant after ultracentrifugation, HTRA1 ΔPDZ S328A was found in the pellet after incubation with full-length or MTBD tau fibrils. As HTRA1 ΔPDZ S328A was soluble after incubation in the disintegration buffer (Supplementary Fig. 8a, c lower panels), this was not due to buffer induced precipitation. More likely, HTRA1 ΔPDZ S328A binds to and co-sediments with fibrils.

Proteolysis of fibrils by HTRA1 was only slightly enhanced by preincubation with HTRA1 S328A ΔPDZ (Fig. 6c). Note, that in the presence of high concentrations of HTRA1 S328A proteolytic products appear with an apparent molecular mass of ca. 25 kDa, possibly due to proteolysis of HTRA1 S328A by HTRA1 (Fig. 6c, asterisk). According to the minor effect of HTRA1 ΔPDZ S328A detected by SDS-PAGE, mass spectrometry revealed that proteolytic cleavage of the tightly packed fibril core was enhanced by preincubation with HTRA1 S328A ΔPDZ to a lesser extent compared to

preincubation with HTRA1 S328A (Fig. 6d). While preincubation with HTRA1 S328A increased the number of cleavage sites significantly in core sections E, F and G, preincubation with HTRA1 ΔPDZ S328A increased the number of cleavage sites in section E only. Changes in the number of cleavage sites in soluble tau were only significant in one, non-core segment of tau (for a detailed list of p-values, see Supplementary Table 1).

Using the cellular model of tau aggregation (Fig. 2), we compared the effects of added HTRA1 ΔPDZ S328A with HTRA1 S328A. As expected, deletion of the PDZ domain of HTRA1 reduced HTRA1's ability to lower the aggregate burden as the amounts of sarkosyl insoluble tau detected in cells treated with HTRA1 ΔPDZ S328A was not significantly reduced compared to the PBS control. Accordingly, the differences between HTRA1 S328A and HTRA1 ΔPDZ S328A and between HTRA1 S328A and PBS control were statistically significant (Supplementary Fig. 8e). Moreover, ITC measurements using the tau derived peptide KTDHGAEIV (aa 385-393) failed to detect binding to HTRA1 lacking the PDZ domain (Fig. 6f, middle panel), while binding to the isolated PDZ domain occurred with a K_D of 50.5 μM (Fig. 6f, left panel) i.e. with similar affinity compared to wt HTRA1 (Supplementary Fig. 7). Taken together, these data indicate that fibril disintegration is impaired but not completely abolished upon PDZ domain deletion, and even though the PDZ domain binds to tau peptides, it needs to be tethered to the protease domain to contribute to fibril disintegration.

Disintegration of amyloidogenic Aβ_{1-42} aggregates

The combination of disintegration and protease activities in HTRA1 could represent a general mechanism allowing cells to tackle other amyloid aggregates as well. To

initially test this model, aggregates of the amyloidogenic $A\beta_{1-42}$ peptide were prepared *in vitro*[32] and incubated with HTRA1 S328A or the control protein MDH, followed by sedimentation assays. As seen with tau fibrils (Fig. 1), incubation with HTRA1 S328A led to soluble $A\beta_{1-42}$ peptides whereas incubation with MDH did not (Supplementary Fig. 9). Note that degradation of Aβ aggregates by HTRA1 has been reported previously[20].

DISCUSSION

We report detailed insights into the mechanism of fibril proteolysis by HTRA1. This conserved protein quality factor has evolved an intrinsic ability, termed disintegration, to destabilize the tightly packed aggregate core to make it accessible to the proteolytic site. The proteolytic mechanism comprises the combined activity of disintegration and peptide bond hydrolysis and thereby ensures efficient degradation of tightly packed fibrils by a single protein quality control factor.

The effect of disintegration by HTRA1 is specific for fibrillar tau because proteolytic degradation of soluble tau is not improved. This excludes substrate independent effects of proteolytically inactive HTRA1, and underlines the challenge imposed by aggregates on the protease for efficient degradation, which is overcome by disintegration. Interestingly, a 10 fold increase of the concentration of active HTRA1 does not affect degradation of soluble tau while fibrils are degraded even faster than soluble tau. This points at distinct enzymatic states and conformation-specific recognition of substrates. This curious observation requires further studies to elucidate the underlying mechanism.

Further specificity exists on the level of primary amino acid sequence as ITC data indicate that not every tau peptide is bound with the same affinity to HTRA1. This

result is based on sequence specific binding pockets of the protease and the PDZ domains of HtrA proteases[33-36]. It is also well established that both, protease and PDZ domains bind substrates in β-strand conformation[7,33], making these sites suitable docking platforms for fibrils that are rich in β-strands. As the PDZ domain is tethered to the protease domain of HTRA1 via a flexible peptide linker it might be instrumental in destabilizing tightly packed fibrils by providing HTRA1 with a flexible substrate binding module distant from the active site. Indeed, all disintegration assays showed that deletion of this domain severely impaired the destabilization of tau fibrils *in vitro* and in cultured cells. The N-terminal domain of HTRA1 was not included in our analyses as biochemical and structural studies suggested it "has no apparent effect on protease activity, and in accordance with the structure-based predictions, neither the IGFBP nor Kazal-like module retains the function of their prototype proteins"[37]. Moreover, a recent report shows that the N-terminus contributes to increased autoproteolysis under reducing conditions and that the autolytic forms display similar activity compared to full-length HTRA1[38].

The proteolytic mechanism of HTRA1 towards fibrils is a specific protein quality control function that is initiated along the entire length of amyloid fibrils, comprises disintegration of tightly packed regions, which is enhanced by the binding of specific sequences by the C-terminal PDZ domain, and ultimately results in the efficient proteolytic removal of amyloid fibrils. The latter step ensures unidirectionality of this process, as proteolytic processing by the same factor eliminates the need of releasing bound substrate, which is ATP dependent in classic chaperonins. Also, proteolysis generates short peptides with a presumably lower affinity to peptide binding sites, therefore allowing dissociation of ligands from HTRA1 in an ATP-independent manner. ATP-independent disaggregation was reported in other systems e.g. the 38-

kDa subunit of the multiprotein chloroplast signal recognition particle reverses aggregation of secretory proteins[39]. Interestingly, here, substrates are not proteolyzed but removed from the equilibrium by secretion into a different cellular compartment. The composite mechanism of fibril proteolysis expands the repertoire of HtrA functions. It has been previously established that the combination of protein refolding and degradation is occurring within single HtrA proteins[40-42]. It is therefore not surprising that some HtrA proteases have disintegration activity as well. Moreover, various functions of the PDZ domain have been characterized in detail, illustrating the evolutionary plasticity of individual domains and regulatory mechanisms within a protein family. The evolution of a mechanism specifically targeting amyloid fibrils including a role of the PDZ domain in disintegrating aggregates contribute to the versatility of HtrA proteins in protein quality control.

Molecular chaperones and conformation specific proteases are key elements of protein quality control pathways that mediate cellular responses against amyloid accumulation, a hallmark of various neurological disorders. Indeed, HSP70 and HSP90 were shown to counteract tau accumulation and neurodegeneration in disease models[43] perhaps by keeping tau soluble[44] and HSP104 was shown solubilize tau fibrils in the test tube[45]. In addition to dedicated chaperones, several proteases are involved in tau degradation including calpain and the proteasome, although the latter can be overwhelmed or inhibited by tau fibrils (for review see[46,47]). In contrast to these factors, HTRA1 employs a unique mechanism of proteolysis including the combination of two functions in one protein, i.e. disintegration and hydrolysis, providing a novel mechanism of counteracting protein aggregation in an ATP-independent manner. As HTRA1 dissolves $A\beta_{1-42}$ aggregates as well, its disintegration activity might have wider implications. This notion is supported by

previous studies describing an association of HTRA1 with various amyloids[20,48]. Moreover, we show here that HTRA1 is internalized by cells from the medium, which might allow its distribution into areas of tissues that have low levels of this protein quality control factor. This feature might even contribute to a delay of onset of folding diseases such as AD. In addition, extracellular HTRA1 could degrade extracellular amyloids and might thus contribute to limited spreading of tau aggregation across brain regions which has been shown to proceed in a prion-like manner[49]. Additional experimental evidence supporting the potential implications of HTRA1 in AD includes the degradation of extracellular Aβ peptides[20], its upregulation in an AD mouse model involving the overproduced Swedish variant of amyloid precursor protein[50] and the inverse correlation of pathological tau and HTRA1 levels in patient brains[26]. Therefore, future work on HTRA1 is likely to contribute to a deeper mechanistic and functional understanding of the various strategies nature has evolved to counteract protein misfolding and aggregation to ultimately delay the onset of protein folding diseases.

ACKNOWLEDGEMENTS

We thank Nina Schulze and Melanie Graessl for help with TIRFM, Daniel Grum and Melisa Merdanovic with ITC, Svenja Blaskowski with mass spectrometry and Vanda Lux for providing purified PDZ domain and Maike Breiden for providing tau. This work was supported by grants EH 100/14-1 (to M.E.) and SFB 1093 (to M.E., M.K. and B.S.) and INST 20876/127-1 FUGG (to M.K.) from Deutsche Forschungsgemeinschaft. The IMP is funded by Boehringer Ingelheim.

AUTHOR CONTRIBUTIONS

S.P., designed and carried out experiments, analyzed data and wrote the paper; A.S and B.S. carried out AFM; F.K. and M.K., carried out mass spectrometry; C.G. and S.R. carried out EM; T.C., performed biochemistry; M.E., outlined the work and wrote the paper.

REFERENCES

1. Wang, L. Towards revealing the structure of bacterial inclusion bodies. *Prion* **3**, 139-145 (2009).
2. Friedman, R. Aggregation of amyloids in a cellular context: modelling and experiment. *Biochem J.* **438**, 415-426 (2011).
3. Akerfelt, M., Morimoto, R.I. & Sistonen, L. Heat shock factors: integrators of cell stress, development and lifespan. *Nat. Rev. Mol. Cell Biol.* **11**, 545-555 (2010).
4. Saibil, H. Chaperone machines for protein folding, unfolding and disaggregation. *Nat. Rev. Mol. Cell Biol.* **14**, 630-642 (2013).
5. Clausen, T., Southan, C. & Ehrmann, M. The HtrA family of proteases. Implications for protein composition and cell fate. *Mol. Cell* **10**, 443-455 (2002).
6. Clausen, T., Kaiser, M., Huber, R. & Ehrmann, M. HTRA proteases: regulated proteolysis in protein quality control. *Nat. Rev. Mol. Cell Biol.* **12**, 152-162 (2011).
7. Truebestein, L. et al. Substrate-induced remodeling of the active site regulates human HTRA1 activity. *Nat. Struct. Mol. Biol.* **18**, 386-388 (2011).
8. Chien, J. et al. Serine protease HtrA1 associates with microtubules and inhibits cell migration. *Mol. Cell Biol.* **29**, 4177-4187 (2009).
9. Tiaden, A.N. & Richards, P.J. The emerging roles of HTRA1 in musculoskeletal disease. *Am. J. Pathol.* **182**, 1482-1488 (2013).
10. Jones, A. et al. Increased expression of multifunctional serine protease, HTRA1, in retinal pigment epithelium induces polypoidal choroidal vasculopathy in mice. *Proc. Natl. Acad. Sci. USA* **108**, 14578-14583 (2011).
11. Vierkotten, S., Muether, P.S. & Fauser, S. Overexpression of HTRA1 leads to ultrastructural changes in the elastic layer of Bruch's membrane via cleavage of extracellular matrix components. *PLoS ONE* **6**, e22959 (2011).
12. Grau, S. et al. The role of human HtrA1 in arthritic disease. *J. Biol. Chem.* **281**, 6124-6129 (2006).
13. Tsuchiya, A. et al. Expression of mouse HtrA1 serine protease in normal bone and cartilage and its upregulation in joint cartilage damaged by experimental arthritis. *Bone* **37**, 323-336 (2005).
14. Chamberland, A. et al. Identification of a novel HtrA1-susceptible cleavage site in human aggrecan: evidence for the involvement of HtrA1 in aggrecan proteolysis in vivo. *J. Biol. Chem.* **284**, 27352-27359 (2009).
15. Campioni, M. et al. The Serine Protease HtrA1 Specifically Interacts and Degrades the Tuberous Sclerosis Complex 2 Protein. *Mol. Cancer Res.* **8**, 1248-1260 (2010).
16. Clawson, G.A., Bui, V., Xin, P., Wang, N. & Pan, W. Intracellular localization of the tumor suppressor HtrA1/Prss11 and its association with HPV16 E6 and E7 proteins. *J. Cell. Biochem.* **105**, 81-88 (2008).
17. Chien, J., He, X. & Shridhar, V. Identification of tubulins as substrates of serine protease HtrA1 by mixture-based oriented peptide library screening. *J. Cell. Biochem.* **107**, 253-263 (2009).
18. Chien, J., Campioni, M., Shridhar, V. & Baldi, A. HtrA serine proteases as potential therapeutic targets in cancer. *Curr. Cancer Drug Targets* **9**, 451-468 (2009).

19. Yang, Z. et al. A variant of the HTRA1 gene increases susceptibility to age-related macular degeneration. *Science* **314**, 992-993 (2006).
20. Grau, S. et al. Implications of the serine protease HtrA1 in amyloid precursor protein processing. *Proc. Natl. Acad. Sci. USA* **102**, 6021-6026 (2005).
21. Milner, J.M., Patel, A. & Rowan, A.D. Emerging roles of serine proteinases in tissue turnover in arthritis. *Arthritis Rheum.* **58**, 3644-3656 (2008).
22. Hara, K. et al. Association of HTRA1 mutations and familial ischemic cerebral small-vessel disease. *N. Engl. J. Med.* **360**, 1729-1739 (2009).
23. Gamblin, T.C. et al. Caspase cleavage of tau: linking amyloid and neurofibrillary tangles in Alzheimer's disease. *Proc. Natl. Acad. Sci. USA* **100**, 10032-10037 (2003).
24. Wang, Y.P., Biernat, J., Pickhardt, M., Mandelkow, E. & Mandelkow, E.M. Stepwise proteolysis liberates tau fragments that nucleate the Alzheimer-like aggregation of full-length tau in a neuronal cell model. *Proc. Natl. Acad. Sci. USA* **104**, 10252-10257 (2007).
25. Spillantini, M.G. & Goedert, M. Tau pathology and neurodegeneration. *Lancet Neurol.* **12**, 609-622 (2013).
26. Tennstaedt, A. et al. Human High Temperature Requirement Serine Protease A1 (HTRA1) Degrades Tau Protein Aggregates. *J. Biol. Chem.* **287**, 20931-20941 (2012).
27. Li, W. & Lee, V.M. Characterization of two VQIXXK motifs for tau fibrillization in vitro. *Biochemistry* **45**, 15692-15701 (2006).
28. Bibow, S. et al. The dynamic structure of filamentous tau. *Angew. Chem. Int. Ed. Engl.* **50**, 11520-11524 (2011).
29. Crowther, R.A. Straight and paired helical filaments in Alzheimer disease have a common structural unit. *Proc. Natl. Acad. Sci. USA* **88**, 2288-2292 (1991).
30. Guo, J.L. & Lee, V.M. Seeding of normal Tau by pathological Tau conformers drives pathogenesis of Alzheimer-like tangles. *J. Biol. Chem.* **286**, 15317-15331 (2011).
31. Mukrasch, M.D. et al. Structural polymorphism of 441-residue tau at single residue resolution. *PLoS Biol.* **7**, e34 (2009).
32. Kuperstein, I. et al. Neurotoxicity of Alzheimer's disease Abeta peptides is induced by small changes in the Abeta42 to Abeta40 ratio. *EMBO J.* **29**, 3408-3420 (2010).
33. Wilken, C., Kitzing, K., Kurzbauer, R., Ehrmann, M. & Clausen, T. Crystal structure of the DegS stress sensor: How a PDZ domain recognizes misfolded protein and activates a protease domain. *Cell* **117**, 483-494 (2004).
34. Krojer, T. et al. Interplay of PDZ and protease domain of DegP ensures efficient elimination of misfolded proteins. *Proc. Natl. Acad. Sci. USA* **105**, 7702-7707 (2008).
35. Meltzer, M. et al. Allosteric activation of HtrA protease DegP by stress signals during bacterial protein quality control. *Angew. Chem. Int. Ed. Engl.* **47**, 1332-1334 (2008).
36. Merdanovic, M. et al. Determinants of structural and functional plasticity of a widely conserved protease chaperone complex. *Nat. Struct. Mol. Biol.* **17**, 837-843 (2010).
37. Eigenbrot, C. et al. Structural and functional analysis of HtrA1 and its subdomains. *Structure* **20**, 1040-1050 (2012).

38. Risor, M.W. et al. The autolysis of human HtrA1 is governed by the redox state of its N-terminal domain. *Biochemistry* **53**, 3851-3857 (2014).
39. Jaru-Ampornpan, P. et al. ATP-independent reversal of a membrane protein aggregate by a chloroplast SRP subunit. *Nat. Struct. Mol. Biol.* **17**, 696-702 (2010).
40. Spiess, C., Beil, A. & Ehrmann, M. A temperature-dependent switch from chaperone to protease in a widely conserved heat shock protein. *Cell* **97**, 339-347 (1999).
41. Krojer, T. et al. Structural basis for the regulated protease and chaperone function of DegP. *Nature* **453**, 885-890 (2008).
42. Malet, H. et al. Binding of substrate proteins inside the molecular cage of the chaperone-protease DegQ. *Nat. Struct. Mol. Biol.* **19**, 152-157 (2012).
43. Miyata, Y., Koren, J., Kiray, J., Dickey, C.A. & Gestwicki, J.E. Molecular chaperones and regulation of tau quality control: strategies for drug discovery in tauopathies. *Future Med. Chem.* **3**, 1523-1537 (2011).
44. Dou, F. et al. Chaperones increase association of tau protein with microtubules. *Proc. Natl. Acad. Sci. USA* **100**, 721-726 (2003).
45. DeSantis, M.E. et al. Operational plasticity enables hsp104 to disaggregate diverse amyloid and nonamyloid clients. *Cell* **151**, 778-793 (2012).
46. Johnson, G.V. Tau phosphorylation and proteolysis: insights and perspectives. *J. Alzheimers Dis.* **9**, 243-250 (2006).
47. Hegde, A.N. & Upadhya, S.C. Role of ubiquitin-proteasome-mediated proteolysis in nervous system disease. *Biochim. Biophys. Acta* **1809**, 128-140 (2011).
48. Karring, H. et al. Composition and proteolytic processing of corneal deposits associated with mutations in the TGFBI gene. *Exp. Eye Res.* **96**, 163-170 (2012).
49. Hardy, J. & Revesz, T. The spread of neurodegenerative disease. *N. Engl. J. Med.* **366**, 2126-2128 (2012).
50. Searcy, J.L., Le Bihan, T., Salvadores, N., McCulloch, J. & Horsburgh, K. Impact of age on the cerebrovascular proteomes of wild-type and Tg-SwDI mice. *PLoS One* **9**, e89970 (2014).

FIGURE LEGENDS

Figure 1

Disintegration of tau Fibrils by HTRA1 S328A. (a) *Sedimentation assay of tau fibrils.* Left panel: 4R tau fibrils were incubated with equimolar amounts of proteolytically inactive HTRA1 S328A (HTRA1 SA) or aldolase control followed by ultracentrifugation. Subsequently, samples before centrifugation (T, total), of pellet (P) and supernatant (S) fractions were subjected to SDS-PAGE and Coomassie staining. Right panel: SDS-PAGE of proteins incubated without tau. Uncropped gel images are provided in a Supplementary Data File. (b, c) *AFM of 4R tau fibrils.* To measure disintegration, fibrillar tau was incubated with equimolar amounts of (b) HTRA1 S328A or (c) the PDZ domain of HTRA1 as in (a) followed by AFM. Representative images are shown. Scale bar, 0.5 μm. For quantification of fibril disintegration, see Supplementary Fig. 1 and 2.

Figure 2

Cell culture model of tau aggregation and sarkosyl extraction of HA-tagged tau. (a) Aggregation of cytoplasmic tau was induced by seeding with MTBD fibrils in 293T HEK cells transiently overexpressing HA-tagged P301L tau. Fixed cells were stained with the amyloid specific fluorescent dye Thioflavin S (ThS, green) and immunostained against the HA tag of overexpressed tau (αHA, red). (b) Cells containing seeded tau filaments were treated with AlexaFluor 568 labeled HTRA1 S328A (1.35 μM) or the dye alone (both shown in red) followed by ThS staining (green) and ToPro3 nuclear counterstaining (blue). Arrowheads indicate regions of distinct colocalization of labeled HTRA1 and tau aggregates. Scale bars, 10 μm. (c)

Cells treated with PBS or seeded with MTBD fibrils were treated with recombinant HTRA1 S328A (4.1 μM) or PBS for 20 h. Lysates were sarkosyl extracted to assess the amounts of soluble (left panel) versus aggregated (middle panel) tau using α tau antibodies. Sarkosyl soluble fractions were also immunoblotted against HTRA1 to show internalization of recombinant HTRA1 (right panel). Actin levels are loading controls or show that sarkosyl pellets did not contain cytoplasmic proteins (middle panel). Recombinant HTRA1 migrates at 37 kDa and native HTRA1 at 51 kDa. For uncropped blots see Supplementary Data File.

Figure 3

Enhanced proteolysis of tau fibrils. (a) Tau fibrils were incubated with proteolytically active HTRA1 (wt HTRA1) after 2 h of preincubation with buffer (left panel), with 10 fold molar excess of HTRA1 S328A compared to proteolytically active HTRA1 (right panel), or with 10 fold molar excess of the isolated PDZ domain of HTRA1 as control (bottom panel). Aliquots were taken before disintegration (-2 h) or at the indicated time points after adding wt HTRA1. (b) Repeated experiments with soluble tau. All samples were subjected to SDS-PAGE and silver staining (n=3). (c) Enhanced proteolysis after disintegration assessed by AFM. Tau fibrils were incubated with buffer, HTRA1 S328A (SA) or the PDZ domain (PDZ) of HTRA1 for 2 h before adding buffer (Ctrl) or active HTRA1 (WT HTRA1) and further incubation for 3 h. Protein concentrations and molar ratios were as in Fig. 3a. The quantification of the abundance of tau fibrils was done as in Fig. 1. Scale bars, 0.5 μm. For representative images, see Supplementary Fig. 5b. Uncropped gel images are provided in a Supplementary Data File.

Figure 4

Association of HTRA1 with fibrils and their proteolysis analyzed by single molecule approaches. (a) Negative-stain electron microscopy of HTRA1 S328A and tau fibrils. Fibrils were incubated with buffer (A), HTRA1 S328A at a molar ratio HTRA1:tau of 1:1 (B) or 3:1 (C) for 20 min before glycerol gradient ultracentrifugation to separate soluble HTRA1 and tau from the fibrils. Representative images from the fractions containing fibrils are shown. The inlets show magnified sections indicating the width of the fibrils as vertical scale bars, i.e. 20 nm (A), 25 nm (B) and 30 nm (C). (b,c) Time-course of proteolysis of tau fibrils followed by TIRFM. DyLight488 labeled tau fibrils (0.01 μM) adhering to the glass bottom of microscopy slides were incubated with (b) buffer or (c) 1 μM wt HTRA1 for 10 h. Images were acquired every 2 h and displayed as single time points (bottom panels) to follow the continuous degradation of fibrils. The local fluorescence decrease is represented as the differences in pixel intensities between t_{0h} and t_{10h}, the values of which were translated into a spectrum LUT (top right). As reference, the respective image of the time point t_{0h} is shown (top left). Scale bars, 5 μm.

Figure 5

Analysis of cleavage sites in tau. (a) Tau fibrils or (b) soluble tau were proteolyzed by wt HTRA1 for the indicated time points following preincubation for 2 h with buffer (orange bars) or a 10 fold molar excess of HTRA1 S328A (green bars). Peptidic cleavage products were analyzed by mass spectrometry. The identified cleavage sites were mapped to sections of the primary sequence of tau indicated at the x-axis of the graphs. The tightly packed core region of tau fibrils is highlighted in red.

Figure 6

Fibril disintegration analyses using HTRA1 S328A and HTRA1 ΔPDZ S328A. (a) Sedimentation assays and (b) AFM measurements were done and analyzed as in Fig. 1. For each condition, >50 individual fibrils recorded by AFM were included into statistical analyses. (c) Proteolytic degradation by wt HTRA1. Tau fibrils were proteolyzed by HTRA1 after preincubation with buffer, 10 x HTRA1 S328A, or 10x HTRA1 ΔPDZ S328A and analyzed as in Fig. 3. * indicates an autoproteolytic product of HTRA1. Uncropped gel images are provided in a Supplementary Data File. (d) Mass-spectrometry as in Fig. 5 using peptidic cleavage products of proteolysis reactions from (c) (n=3). For statistical analysis, see Supplementary Table 1. (e) *Cell based assays* done as in Fig. 2c. For uncropped blots see Supplementary Data File. (f) Binding of the tau peptide KTDHGAEIV (aa 385-393) to the PDZ domain of HTRA1 measured by ITC.

ONLINE METHODS

Antibodies and chemicals

Rabbit polyclonal antibodies against tau and mouse monoclonal antibodies against actin and HA-tag were obtained from Abcam (ab-64193), MP biomedicals (clone C4, #691001) and Covance (HA.11, clone 16B12, cat.no. MMS-101P), respectively. Polyclonal antibody against the HTRA1 PDZ domain (aa377-480)[266] was made in-house and tested for specificity as well as cross-reactivity with other HtrA family members (data not shown). The rabbit polyclonal antibody against residues 158-480 of HTRA1 was a gift from A. Baldi[20]. The $A\beta_{1-42}$ peptide was ordered from Designer BioScience, Cambridge, UK, tau peptides used in ITC binding assays were ordered from Intavis, Cologne. For immunofluorescence microscopy, secondary Alexa Fluor 633 coupled goat anti-mouse and goat anti-rabbit antibodies were purchased from Life Technologies, as was the To-Pro 3 nuclear counterstain. The amine-reactive dye Alexa Fluor 568 carboxylic acid, succinimidyl ester, as well as fluorescently labeled secondary antibodies for immunofluorescence were purchased from Life Technologies. Amine-reactive DyLight488 antibody labeling kits were purchased from Thermo Scientific, glass-bottom slides for TIRFM by Ibidi (Martinsried, Germany). Thioflavin S, the protein transfection reagent Pro-Ject and MDH from porcine heart were ordered from AAT Bioquest, Thermo Fisher Scientific and Roche, respectively. Aldolase was taken from a gel filtration HMW calibration kit (GE Healthcare).

Plasmids

Bacterial expression plasmids based on the pET21d (Novagen) for purification of recombinant 6 x His – tagged HTRA1, ΔPDZ, HTRA1 S328A and S328A ΔPDZ were published previously[7], the expression plasmid encoding the PDZ domain of HTRA1 with a C-terminal 6 x His – tag (aa 380-480) was constructed by PCR and standard cloning techniques using the above plasmid as template. 4R wt and MTBD tau plasmids were constructed by cloning the coding sequence of full-length 2N4R human tau (441 aa isoform) and of aa 258-360 containing the ΔK280 mutation into pET3d expression vectors (Novagen) using *Nco*I and *Bam*HI restriction enzymes. The MTBD fragment was chosen because of its previously published high aggregation propensity[24]. For transient overexpression of HA-tagged full-length 4R tau with the P301L mutation, the respective coding sequence was amplified and cloned into pcDNA3.1 for constitutive overexpression in mammalian cultured cells, using a forward primer introducing an N-terminal HA tag with a *BamH*I restriction site and a reverse primer with an *Xho*I restriction site.

Expression and purification of recombinant human HTRA1, full-length tau and MTBD of tau

For the *in vitro* protease and disintegration assays and the treatment of cells with recombinant HTRA1, the indicated variants of human HTRA1 were purified as described previously[26]. After Ni-NTA affinity and hydroxyapatite chromatography with phosphate gradient elution, the protein was further purified by size exclusion chromatography using Superdex 200 preparation grade columns (GE Healthcare) in 10 mM HEPES, 50 mM $(NH_4)_2SO_4$, pH 7.5. Protein concentrations were determined by Bradford assays and SDS-PAGE. HTRA1, HTRA1 ΔPDZ and the PDZ domain comprise residues 158-480, 158-375 and 377-480, respectively. 4R wt tau and MTBD tau were purified as described previously[26].

Heparin induced fibrillization of recombinant human tau

Aggregation of human full-length tau was performed as described previously[26] with minor modifications. 20 µM tau was incubated in aggregation buffer (100 mM sodium acetate, 2 mM DTT, pH 7) at 55 °C, 800 rpm for 10 min, followed by addition of 1 mM fresh DTT and 50 µM heparin. After fibrillization at 37 °C, 900 rpm for 48 h up to 5 days, with addition of 1 mM of fresh DTT every 24 – 48 h, the extent of aggregation was checked by ultracentrifugation and Thioflavin T fluorescence. The resulting aggregates were used in disintegration experiments as explained above. For the proteolysis experiments with HTRA1, the tau fibrils were sedimented by ultracentrifugation at 186,000 x g, 4 °C for 1 h and resuspended with HTRA1 proteolysis buffer in order to remove heparin and soluble tau species. Concentrations were determined by SDS-PAGE, Coomassie staining and comparison with BSA samples of known concentration. Fibrils composed of MTBD tau were assembled accordingly, except that the duration of fibrillization was reduced to 24 h.

Protein labeling

For immunofluorescence microscopy, recombinant human HTRA1 was labeled with the amine reactive fluorescent dye Alexa Fluor 568 carboxylic acid, succinimidyl ester (Life Technologies), by incubating 200 µM of HTRA1 with 2 mM of the reactive dye in 100 mM sodium bicarbonate, pH 8.3, at room temperature (RT) and constant agitation for 1 h. Prior to the labeling reaction, HTRA1 solution was adjusted to the labeling buffer using desalting columns (PD SpinTrap G-25, GE Healthcare). After completing the labeling reaction, the labeled protein was separated from the free dye using desalting columns and stored at -80 °C in single-use aliquots. For TIRFM of fibrils, tau fibrillization was performed as described above for 48 h, the fibrils were dialyzed against the labeling buffer PBS, pH 7.4, and incubated with 1/10 of the recommended amount of DyLight 488 amine-reactive dye from an antibody labeling kit (Thermo Scientific). Labeling buffer and the ratio of dye to protein were chosen to yield a low degree of labeling in order to preserve the fibril structure and minimize the interference of the label with the proteolysis by HTRA1. The labeling reaction was performed for 1 h at RT without agitation in the dark. The labeled fibrils were dialyzed against PBS, pH 7.4 to remove unbound dye and stored on ice in the dark until usage.

Disintegration of tau fibrils by HTRA1 *in vitro*

For disintegration assays by ultracentrifugation, 6.8 µM full-length or MTBD tau aggregates from 48 h or 24 h fibrillization reactions, respectively, were incubated with buffer or amounts of HTRA1 S328A corresponding to the indicated molar ratios or with control proteins in 100 mM piperazine-N,N′-bis(2-ethanesulfonic acid) (PIPES), 100 mM NaCl, 1 mM DTT, pH 7 at 37 °C, 450 rpm, for 16 h. The titration of HTRA1 was done in 100 mM 2-(*N*-morpholino)ethanesulfonic acid (MES), 100 mM NaCl, 1 mM DTT, pH 6 for 1 h. Analysis of solubility was performed by ultracentrifugation of 20 µl samples at 186,000 x g, 4 °C for 1 h. As controls, HTRA1 or the proteins indicated were incubated under the same conditions without tau, but with the respective volume of aggregation buffer (100 mM sodium acetate, 2 mM DTT, pH 7). The supernatants were mixed with loading buffer containing DTT, the pellets were solubilized with the respective amounts of loading buffer by thorough vortexing and resuspending. Total samples were removed before ultracentrifugation and treated accordingly. The amounts of tau in the individual fractions were assessed

by SDS-PAGE followed by Coomassie staining. MTBD tau was detected by immunobloting with a polyclonal antibody against the repeat region of tau, whereas HTRA1 and control proteins were analyzed by Coomassie staining. The relative amounts of soluble Tau were determined by calculating the ratio of band intensities of the supernatant versus total protein samples using the ImageJ gel analysis plugin. For the titration experiments using varying concentrations of HTRA1, HTRA1 S328A was incubated with full-length tau fibrils at the indicated ratios for 1 h at 37°C followed by ultracentrifugation and SDS-PAGE as described above. Band intensities determined using the gel analyzing tool implemented in ImageJ of Coomassie stained gels of the supernatant samples were divided by the intensities of the total samples for the relative amount of solubilized tau shown in the graph. 4-8 independent experiments were used to calculate the mean and SEM of solubilized tau for each ratio. For AFM analysis, the disintegration was done using 100 mM MES, 100 mM NaCl, 1 mM DTT, pH 6 and the disintegration samples were diluted to 2 µM final tau concentration based on the full-length monomer molecular weight of 45.8 kDa.

Preparation of $A\beta_{1-42}$ aggregates and disintegration by HTRA1 S328A

For the aggregation of the $A\beta_{1-42}$ peptide, the lyophilized powder was dissolved in DMSO to obtain a 10 mM $A\beta_{1-42}$ stock solution which was stored as 20 µl aliquots at -20°C. The aggregation was performed as described in the article text, by dilution of the $A\beta_{1-42}$ peptide into aggregation buffer (50 mM Tris, 50 mM NaCl, 1 mM EDTA, pH 7.5) to a final concentration of 50 µM, followed by incubation without agitation at 37°C for 14 h. The successful aggregation was assessed by means of ThT fluorescence and sedimentation by ultracentrifugation. $A\beta_{1-42}$ disintegration was performed by incubation of 25 µM $A\beta_{1-42}$ aggregates with equimolar amounts of HTRA1 S328A or MDH in 100 mM MES, 100 mM NaCl, pH 6 at 37 °C, 450 rpm for 16 h. After the incubation period, the insolubility was determined by ultracentrifugation, followed by SDS-PAGE of a sample from the disintegration reaction, the supernatant and the pellet using pre-cast 4-12% Bis-Tris gels (Life Technologies). The protein bands were detected by silver staining.

***In vitro* proteolysis of soluble and fibrillar tau**

Proteolysis of tau fibrils and soluble tau by HTRA1 was done essentially as described in the article text. 680 nM tau were incubated with wt HTRA1 at a molar protease:substrate ratio of 1:2.5, i.e., with 272 nM wt HTRA1 in 50 mM Tris/HCl, 5 mM Tris(2-carboxyethyl)phosphine (TCEP), pH 8 at 37 °C, 350 rpm. Aliquots were taken at the indicated time points, mixed with loading dye and 50 mM TCEP, flash frozen in liquid nitrogen and kept frozen until analysis by SDS-PAGE. For disintegration followed by proteolysis, tau fibrils or soluble tau were incubated with a 10 fold molar excess of HTRA1 S328A, S328A ΔPDZ or the PDZ domain as compared to wt HTRA1 (i.e., 2.72 µM) or buffer at 37 °C for 2 h before addition of wt HTRA1. Samples were boiled at 96 °C for 10 min and subjected to SDS-PAGE using pre-cast 10% Bis-Tris polyacrylamide gels (Life Technologies). For proteolysis followed by AFM, the same protocol was used except that 2 µM fibrillar tau was used, with the other protein concentrations adjusted accordingly to obtain the same molar ratios. Before AFM, the ultracentrifugation step was omitted in order to keep the fibrils intact for reliable analysis.

AFM and image analysis

Without previous treatment, 5 µl samples were deposited on a freshly cleaved mica surface (Plano GmbH) and adsorbed for 3 min at RT. After addition of 15 µl 1X TAEMg (40 mM Tris, 20 mM acetic acid, 2 mM EDTA, 12.5 mM Mg acetate, pH 8), the sample was scanned on a MultiModeTM 8 microscope (Bruker, Germany) equipped with a Nanoscope V controller, using the ScanAsyst® PeakForce TappingTM operational mode. Silicon nitride probes with 0.7 N/m nominal spring constant and sharpened pyramidal tips (ScanAsyst Fluid+, Bruker) were used for scanning. At least three images (3x3 µm) were acquired from random locations of the mica surface for statistical analysis of the results. Recorded views were 3rd order flattened and exported as TIFF files using the NanoScope 6.14 software (Bruker). Fibril lengths were analyzed with imageJ [51] by creating a collection of regions of interest (ROIs) corresponding to individual fibrils using the freehand selection tool and measuring the sets of ROIs of individual images. The sums of the lengths of fibrils in the images of each sample were statistically analyzed employing the two-sided t-test for unpaired samples with Welch's correction using the statistical analysis software Prism 5 (GraphPad). To detect possible changes in the abundance of fibrils depending on their individual lengths, the frequency distribution was analyzed with the same statistical software, using the data sets obtained as described above. The bin width for the distribution was set to 50 nm, and the distribution of lengths ranging from 0-1200 nm was displayed as absolute numbers or relative frequencies of fibrils populating each length interval.

Negative-stain electron microscopy of tau fibrils bound by HTRA1 S328A

Fibril decoration with HTRA1 and isolation. Before isolation via glycerol gradient ultracentrifugation and negative-stain EM, 12 µM tau fibrils were incubated in 300 µl 50 mM Tris, pH 8, with HTRA1 at a molar ratio HTRA1:tau of 1:1 or 3:1 or with buffer at 37°C for 20 min. Glycerol gradients (10-40% (vol/vol)) were prepared using a gradient former (Gradient master 107, Biocomp). Subsequently, samples were added on the top of the gradients and were then centrifuged using a SW40-Ti rotor (Beckman Instruments) at 40,000 x g (i.e., 285,000 x g), 4°C, for 16 h. Fractions were harvested and analyzed by EM.

Grid preparation and image recording. 4 µl sample droplets were applied to freshly glow-discharged grids (Agar scientific; G2400C) covered by a continuous thin carbon film. The sample was left for 45sec on the grid before blotting using filter paper (Whatman no. 4). The grid was then washed twice with ddH2O and negatively stained with 0.7% uranyl formate (Polysciences) for 45 sec. After blotting the grid was air-dried and transferred to a JEOL JEM-1400 electron microscope equipped with a LaB6 and operated at 120 kV. Digital micrographs were recorded with a 4k x 4k CMOS Camera F416 (TVIPS) using minimal dose conditions

Total Internal Reflection Fluorescence Microscopy (TIRFM) of labeled fibrils

Preparation of microscopy slides and image acquisition. For the visualization of the time-course of the proteolytic degradation of tau fibrils by HTRA1 using TIRF microscopy, heparin induced tau fibrils were labeled with a DyLight 488 fluorescent dye as described above. Sterile 8-well glass bottom microscopy slides (Ibidi, Martinsried, Germany) were coated with the labeled fibrils by incubation of 0.01 µM tau fibrils diluted in 50 mM Tris/HCl, pH 8, at 37°C protected from light for 1 h. After the coating reaction, the dishes were washed 3 x with PBS, pH 7.4 prior to the addition of 1 µM wt HTRA1 in 50 mM Tris/HCl, 5 mM TCEP, pH 8, or buffer alone. For the generation of movies, 120 images were recorded over a time period of 4 h, for

the quantification of the fluorescence decrease, higher resolution images were recorded every 2 h for a total of 10 h. To visualize the decrease in fluorescence irrespective of bleaching, the coated dishes were incubated with HTRA1 or buffer for 14 h before recording single high resolution endpoint images. All TIRFM experiments were performed on an Eclipse Ti-E (Nikon) inverted microscope operated by the AndorIQ image acquisition software and equipped with an Andor AOTF Laser Combiner (Andor Technology), a motorized TIRF Illuminator Unit (Nikon) and a Clara Interline CCD camera (Andor Technology). The images were acquired using the 488 nm laser line and an Apo TIRF 100x/1.49NA oil-immersion objective (Nikon).

Data processing. All image processing and quantification of the raw data acquired as described above was performed with ImageJ[51]. All time series of images were registered using the StackReg Plugin[52] and normalized to the same range of minimum and maximum displayed values prior to further analysis and processing. The movies were exported as .avi files at a frame-rate of 24 frames per second and JPEG compression. Regions of interest (ROIs) from the 10 h time series were displayed as a series of time points or used for the generation of fluorescence difference images. The latter were created by displaying the difference of the intensities of each pixel value between the t_{0h} and t_{10h} images as 8-bit images using the spectrum lookup table (LUT). For the analysis of local proteolysis depending on the relative position along the fibril length, 45 randomly chosen fibrils were analyzed with ImageJ. Single fibrils were marked with the freehand drawing tool, and their pixels were assigned to five portions of equal size corresponding to relative positions along the fibril. The fluorescence decrease in each portion relative to the total fluorescence decrease of the fibril was included in the data analysis. In order to quantify the changes in fluorescence of single fibrils as shown in Supplementary Fig. 6b, ROIs containing fibrils were generated by setting an intensity threshold for the t_{0h} time point. This set of ROIs was applied to all time point images, and the average intensity of each ROI corresponding to a single fibril (or group of fibrils when overlapping) was normalized to the respective starting intensities at time point t_{0h}. Each value shown corresponds to the mean value of 300-400 individual ROIs per sample. The single endpoint images were adjusted to equal intensity ranges and displayed as grayscale images or as images using the spectrum LUT for a more demonstrative visualization of fluorescence intensities.

Mass spectrometry and analysis of cleavage sites

Sample preparation for LC-MS. For the mass spectrometric analysis of cleavage sites by HTRA1, proteolysis of soluble tau and tau fibrils was performed for the indicated duration after 2 h preincubation with HTRA1 S328A or proteolysis buffer. Buffers and concentrations were the same as described above. 20 µl samples were acetone precipitated for 2 h at -80 °C. The supernatant containing the peptidic cleavage products was dried, resuspended with PBS and desalted as described[53].

LC-MS/MS. Experiments were performed on an Orbitrap Elite instrument (Thermo,[54]) that was coupled to an EASY-nLC 1000 liquid chromatography (LC) system (Thermo). The LC was operated in the one-column mode. The analytical column was a fused silica capillary (75 µm × 25 cm) with integrated PicoFrit emitter (New Objective) packed in-house with Reprosil-Pur 120 C18-AQ 3 µm resin (Dr. Maisch). The analytical column was encased by a column oven (Sonation) and attached to a nanospray flex ion source (Thermo). The column oven temperature was adjusted to 45°C during data acquisition. Otherwise the temperature was kept at 30°C. The LC

was equipped with two mobile phases: solvent A (0.1% formic acid, FA, in UPLC grade water) and solvent B (0.1% FA in acetonitrile, ACN). Peptides were delivered directly to the analytical column via the integrated autosampler at a flow rate of 0.7-0.9 µl/min in 100% solvent A. Peptides were subsequently eluted from the column by running a 25 min gradient of solvent A and solvent B (start with 2% B; gradient 2% to 35% B for 10 min; gradient 35% to 45% B for 6 min; gradient 45% to 100% B for 2 min; 100% B for 7 min) at a flow rate of 300 nl/min.

The mass spectrometer was operated using Xcalibur software (version 2.2 SP1.48). The mass spectrometer was set in the positive ion mode. Precursor ion scanning was performed in the Orbitrap analyzer (FTMS) in the scan range of m/z 300-1,800 and at a resolution of 30,000 with the internal lock mass option turned on (lock mass was 445.120025 m/z, polysiloxane)[55]. Product ion spectra were recorded in a data dependent fashion in the ion trap (ITMS) in a variable scan range and at a rapid ~~normal~~ scan rate. The ionization potential (spray voltage) was set to 1.6 – 2.0 kV. Peptides were analyzed using a repeating cycle consisting of a full precursor ion scan (1.0×10^6 ions) followed by seven product ion scans (1.0×10^4 ions) where peptides are isolated based on their intensity in the full survey scan (threshold of 500 counts) for tandem mass spectrum (MS2) generation that permits peptide sequencing and identification. CID collision energy was set to 35% for the generation of MS2 spectra. During MS2 data acquisition dynamic ion exclusion was set to 60 seconds with a maximum list of excluded ions consisting of 500 members and a repeat count of one. Ion injection time prediction, preview mode for the FTMS, monoisotopic precursor selection and charge state screening were enabled. Only charge states bigger than 1 were considered for fragmentation.

Peptide and Protein Identification. The recorded RAW files were processed in ProteomDiscoverer 1.3 (PD13, Thermo). MS2 spectra were extracted using the Spectrum Selector node. Precursor selection was set to "use MS1 precursor". The mass range was set between 350 – 5,000 Da with a minimum peak count of 1. Mass analyzer was set to "any" and MS order to "MS2". Activation type was set to "is CID" and Scan type was defined as "full" with ionization source set to "is nanospray". Selected spectra were submitted to the in house MASCOT server (version 2.4.1[56]) using the PD13 MASCOT node. MS2 spectra data were searched against an *E. coli* K12 reference protein database downloaded from Uniprot (www.uniprot.org/ taxonomy/complete-proteomes, 4,312 protein sequences, download date 25.10.2013) and concatenated with the contaminants database (as implemented in MASCOT, 263 sequences) and the sequences of interest for Tau and HtrA1. The contaminants database contains known MS and was included to estimate the level of contamination. Mascot searches allowed for oxidation of methionine residues (16 Da) but no static modifications (cysteine residues were not alkylated with iodoacetamide). In accordance with our aim to detect endogenous cleavage sites no enzyme was specified. The instrument type was set to ESI-TRAP and the mass tolerance was set to ±5 ppm for precursor mass and ±0.5 Da for product ion masses. MS2 spectra matches were then evaluated using the peptide validation node of PD13 with the standard settings (search against decoy database, target false discovery rate (FDR, strict): 0.01 and target FDR (released): 0.05). The reported results were further filtered. On peptide level only peptides with a minimum confidence 'medium' were reported and on protein level only proteins with a minimum of at least two peptide hits were reported.

Data processing and P-site mapping. For data processing peptide lists were directly downloaded from MASCOT as CSV files. Prior to the download peptides were

filtered based on their peptide score. Only peptides with a stringent score >29 were accepted (identity threshold). The downloaded files were then further processed with several in-house developed PERL scripts. First the CSV files were converted to plain text files using the script MASCOT_Datacon_v05.pl. The obtained text files were then batch processed with the script SVG_builder_FAK_0555_script_v11.pl. Basically this script goes through all indicated peptide lists and records occurrences of peptides in each individual experiment. Also it calculates the start and end position of each peptide in an identified protein match and records the number of peptide spectrum matches (PSM) irrespective of any modifications (count is based only on amino acid sequence). The recorded peptides were mapped to the primary sequence of full-length 4R tau, and the P1 sites were derived from their N- and C-terminal residues. Assignment of the cleavage site to equal sized sections of the tau primary sequence was done with Excel (Microsoft).

Isothermal titration calorimetry (ITC)

To detect the direct interaction between HTRA1, HTRA1 ΔPDZ or the isolated PDZ domain of HTRA1 with tau derived peptides, the indicated proteins were dialyzed against 50 mM Tris, 150 mM NaCl, pH 8 or 100 mM NaH_2PO_4, 150 mM NaCl, pH 7.2. The peptides were dissolved in the same buffer but with 2% DMSO to a final concentration of 2 mM. The measurements were performed with a MicroCal ITC200 (Malvern Instruments) with 2 mM peptide in the syringe and 20 µM or 40 µM protein as indicated in the sample cell. For each measurement, 20 injections á 2 µl were done, except for the first 0.8 µl injection, at 37°C with a stirring speed of 750 rpm. To exclude dilution effects, control measurements using peptide injections into buffer or buffer injections into the sample cells containing HTRA1 were performed. The raw data was evaluated using the MicroCal Origin software and applying the one set of sites fitting mode according to the instructions of the manufacturer.

Internalization of recombinant HTRA1 by 293T HEK cells

Given that HTRA1 is secreted into the cell culture medium but also located to the cytosol, we reasoned that this subfraction of HTRA1 could be reinternalized after secretion. To study the spontaneous internalization of recombinant HTRA1 protein from the medium, 8 x 10^5 293T HEK cells were seeded in poly-D-lysine coated 6 cm cell culture dishes and grown for 24 h to reach 50-60% confluency. Cells were washed twice with PBS before addition of 4 ml serum-free medium containing recombinant, labeled HTRA1 in the concentration and for the incubation time indicated. Subsequently, cells were detached from the culture dish by trypsin / EDTA treatment, centrifuged, and the cell pellet was washed thoroughly with PBS to remove all residual trypsin from the sample. The resulting pellet was lyzed with RIPA buffer containing protease inhibitor (Roche). 150 µg total cell lysate were analyzed by SDS PAGE followed by immunoblotting. Alternatively, 1.5 x 10^5 cells were seeded in each well of a 24 well plate on poly-D-lysine coated glass coverslips, treated with 500 µl serum-free DMEM medium per well containing 50 µg/ml Alexa Fluor 568 labeled HTRA1 S328A, grown for 24 h, washed, methanol fixed and stained for immunofluorescence as described above. As a control for the uptake of labeled HTRA1, the amine reactive dye by itself was saturated by 1:5 dilution with 100 mM Tris, pH 8.42, and the same concentration as assessed by absorption at λ = 578 nm of the labeled protein and isolated dye was used.

Seeding of tau aggregation in 293T HEK cells

The seeding of intracellular tau aggregation in 293T HEK cells was done as described[30] with some modifications and the additional analysis of the effect of HTRA1 internalized from the extracellular space. 293T HEK cells were used, as this cells line is suitable for particularly high expression, which is needed for efficient seeding of cytoplasmic tau aggregation. Cell lines are routinely tested for mycoplasma contaminations on a regular basis in the lab.

Preparation of MTBD aggregate seeds. Fibril seeds composed of MTBD tau were prepared by fibrillization for 24 h as described above, followed by ultracentrifugation at 186,000 x g, 4 °C for 1 h. The pellets were thoroughly resuspended with PBS, pH 7.4, vortexed, and the extent of fibrillization was checked by SDS-PAGE of samples from the supernatant and pellet. Typically, all of the MTBD tau was found in the pellet after 24 h of fibrillization. MTBD tau aggregates were sonicated in a water bath for 2 x 2 min before performing protein transfection.

Transient transfection of 293T HEK cells and seeding of aggregation. For sarkosyl extraction experiments, 293T HEK cells were transiently transfected by nucleofection (Lonza, Switzerland) with a pcDNA3.1 plasmid for overexpression of HA-tagged full-length human tau with the point mutation P301L. 4 x 10^5 cells were grown in each well of a 6-well plate for expression of P301L tau for 24 h to reach about 50% confluency. Cell culture dishes were poly-L-lysine coated prior to seeding. Freshly prepared MTBD tau aggregate seeds were transfected into the cells at a final concentration of 17.5 µg/ml using 10 µl per well of the cationic lipid based protein transfection reagent Pro-Ject, followed by 4 h incubation with DMEM culture medium without serum and 20 h of incubation with 0.5% fetal bovine serum (FBS). For HTRA1 internalization experiments, cells were washed twice with serum-free DMEM medium, followed by addition of 2 ml of medium conditioned with either PBS or HTRA1 at a final concentration of 150 µg/ml, i.e. 4.1 µM, and incubated at 37 °C for 20 h before performing sarkosyl extraction and immunoblotting.

Sarkosyl extraction from cultured cells. After seeded aggregation, sarkosyl extraction was performed to assess the abundance of aggregated versus soluble, HA-tagged P301L tau. Sarkosyl extraction was done essentially as described before [30] with some modifications. Cells were detached from the culture dish by trypsinization and washed thoroughly with PBS to remove all residual trypsin from the cell pellet. The pellet was resuspended with lysis buffer containing sarkosyl, 10 mM Tris/HCl, 150 mM NaCl, 1 mM EGTA, 5 mM EDTA, 1% sarkosyl, pH 7.4 with protease inhibitor (Roche complete protease inhibitor tablet), and incubated on ice for 15 min. For cell lysis, the suspension was 10 x syringe sheared with a 27G needle, followed by incubation on ice for 15 min, 2 x 2 min sonication in the water bath and incubation at 25 °C for 20 min. The samples were ultracentrifuged at 186,000 x g, 4 °C for 60 min, the supernatant was saved as sarkosyl soluble fraction, the pellet was resuspended with the corresponding amount of SDS loading buffer containing 1% SDS by vigorous vortexing. Equal amounts of the individual samples were subjected to SDS-PAGE and immunoblotting based on the sarkosyl supernatant concentrations determined by absorption at 280 nm using a NanoDrop micro volume spectrophotometer (Peqlab, Germany). Volumes of the sarkosyl insoluble fractions were adjusted accordingly. The samples were loaded onto 10% SDS gels followed by immunoblotting against tau, the HA-tag, HTRA1 or actin. The bands were detected by alkaline phosphatase (AP) coupled secondary antibodies, followed by chromogenic detection of AP activity. For quantification, blots from 3-4 independent experiments were used to calculate the signal intensities of Sarkosyl pellet bands from

HTRA1 treated samples relative to the PBS treated samples, using the gel analysis tool implemented in ImageJ.

Immunofluorescence and confocal laser-scanning microscopy

For seeding of tau aggregation and HTRA1 internalization experiments to be analyzed by confocal laser-scanning microscopy, the cells were transfected as done before for sarkosyl extraction except some modifications. Following transfection with tau P301L expression plasmids, 1.6×10^5 cells were transferred to each well of 24 well plates with poly-D-lysine coated glass coverslips and grown for 24 h before transfection with MTBD seeds which were prepared as described above. For transfection in 24 well plates, 2.5 µl of the transfection reagent were used per well. Where indicated, treatment with labeled HTRA1 was done as described above except that 1.35 µM labeled HTRA1 was used in a final volume of 500 µl. After an incubation period of 20 h as described above, cells were fixed with ice-cold methanol, permeabilized with 0.5% Triton X-100 for 5 min, and washed with PBS before further staining was performed. For the detection of amyloid aggregates, Thioflavin S (ThS) staining was performed as described in the article text, by incubation with 0.005% ThS, dissolved in PBS and sterile filtered, for 8 min at RT, followed by 5 x washing with 50% ethanol for 5 min. The samples were then blocked with 5% bovine serum albumin (BSA) for 30 min before antibody staining was done with primary antibodies as indicated, using Alexa Fluor 633 labeled secondary antibodies. The anti HA antibody and secondary antibodies were diluted 1:500, the polyclonal anti HTRA1 PDZ antibody was used in 1:50 dilution in 3% BSA/PBS. Before mounting the samples with ProLong Gold antifade mounting solution (Life Technologies), they were washed with PBS 3 x for 15 min at RT. DAPI was added in 1:10,000 dilution together with the secondary antibody solutions. The nuclear counterstain To-Pro 3 iodide (Life Technologies) was used diluted 1:500 from a 1 mM stock solution. When To-Pro 3 staining was done, the samples were treated with 100 µg/ml RNAse A at 37 °C for 20 min to eliminate unspecific staining of cytoplasmic RNA. Microscopy was done with a Leica TCS SP5 Confocal Laser Scanning Microscope equipped with Leica HyD Gallium Arsenide phosphide hybrid detection systems. Image acquisition was performed with the same detector sensitivity settings for samples and controls. Images of the different channels were acquired individually in serial acquisition mode to avoid fluorescent bleed-through. Images of single focal planes using 60 µm pinhole width are shown.

ONLINE METHODS REFERENCES

51. Schneider, C.A., Rasband, W.S. & Eliceiri, K.W. NIH Image to ImageJ: 25 years of image analysis. *Nat. Methods* **9**, 671-675 (2012).
52. Thevenaz, P., Ruttimann, U.E. & Unser, M. A pyramid approach to subpixel registration based on intensity. *IEEE Trans. Image Process* **7**, 27-41 (1998).
53. Rappsilber, J., Mann, M. & Ishihama, Y. Protocol for micro-purification, enrichment, pre-fractionation and storage of peptides for proteomics using StageTips. *Nat. Protoc.* **2**, 1896-1906 (2007).
54. Michalski, A. et al. Ultra high resolution linear ion trap Orbitrap mass spectrometer (Orbitrap Elite) facilitates top down LC MS/MS and versatile peptide fragmentation modes. *Mol. Cell. Proteomics* **11**, O111 013698 (2012).

55. Olsen, J.V. et al. Parts per million mass accuracy on an Orbitrap mass spectrometer via lock mass injection into a C-trap. *Mol. Cell. Proteomics* **4**, 2010-2021 (2005).
56. Perkins, D.N., Pappin, D.J., Creasy, D.M. & Cottrell, J.S. Probability-based protein identification by searching sequence databases using mass spectrometry data. *Electrophoresis* **20**, 3551-3567 (1999).

Competing financial interests statement

There are no competing financial interests

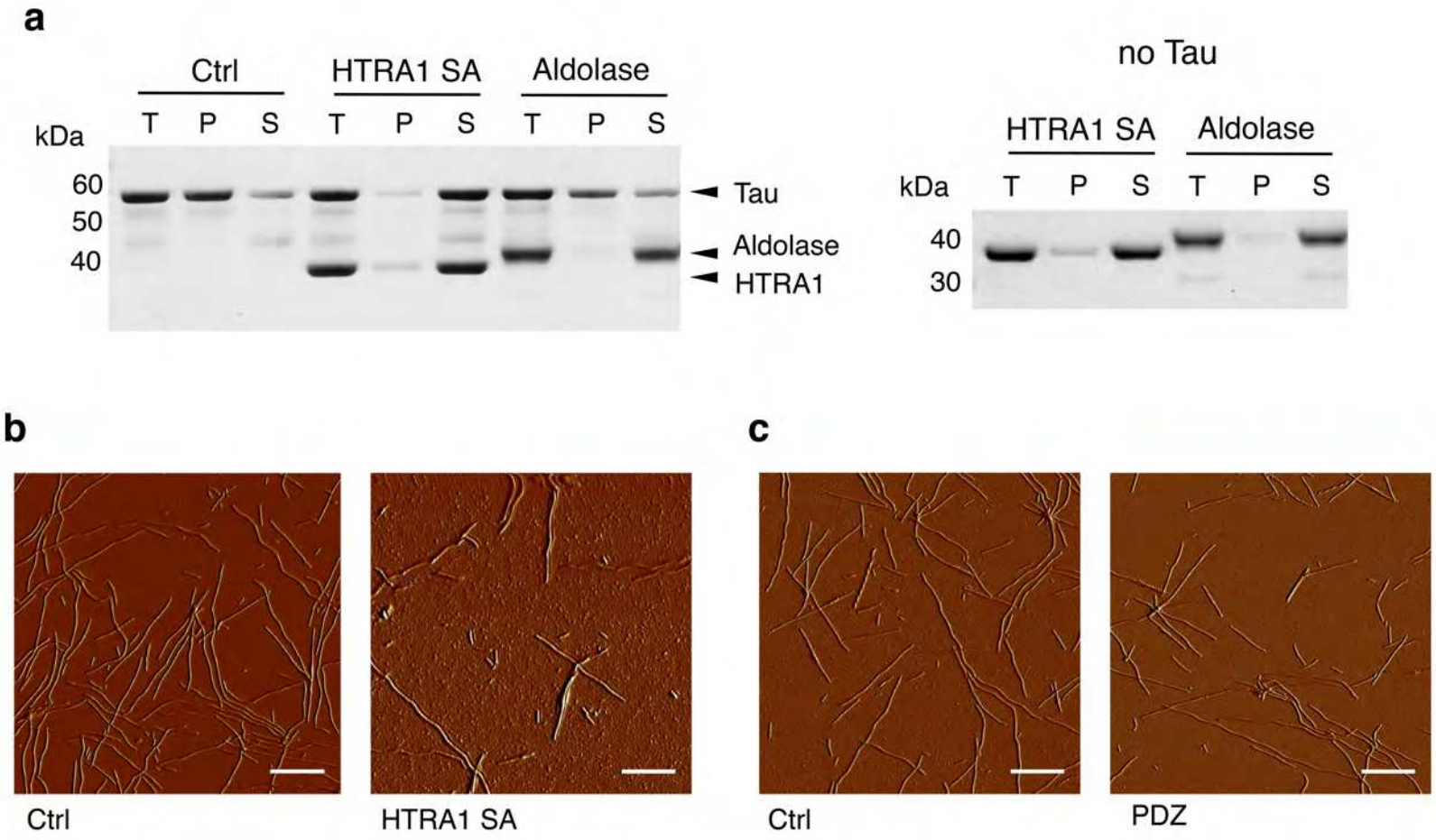
a
Ctrl
HTRA1 SA
Aldolase
T P S T P S T P S
kDa
60
50
40
Tau
Aldolase
HTRA1
no Tau
HTRA1 SA
Aldolase
kDa
T P S T P S
40
30
b
Ctrl
HTRA1 SA
c
Ctrl
PDZ

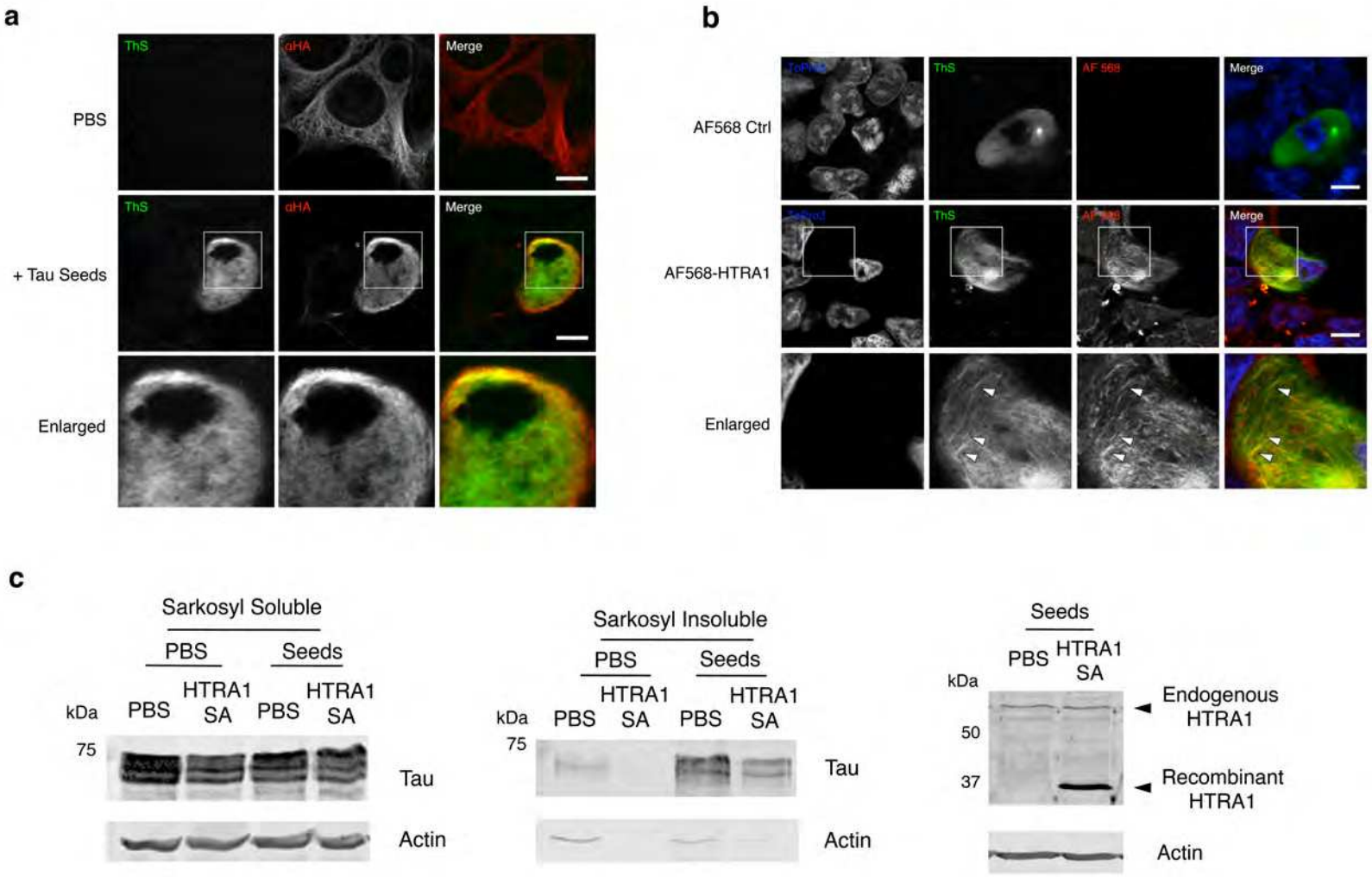
a
PBS
+ Tau Seeds
Enlarged
ThS
αHA
Merge
b
AF568 Ctrl
AF568-HTRA1
Enlarged
ThS
AF 568
Merge
c
Sarkosyl Soluble
PBS
Seeds
kDa
PBS
HTRA1 SA
75
Tau
Actin
Sarkosyl Insoluble
Seeds
50
37
Endogenous HTRA1
Recombinant HTRA1

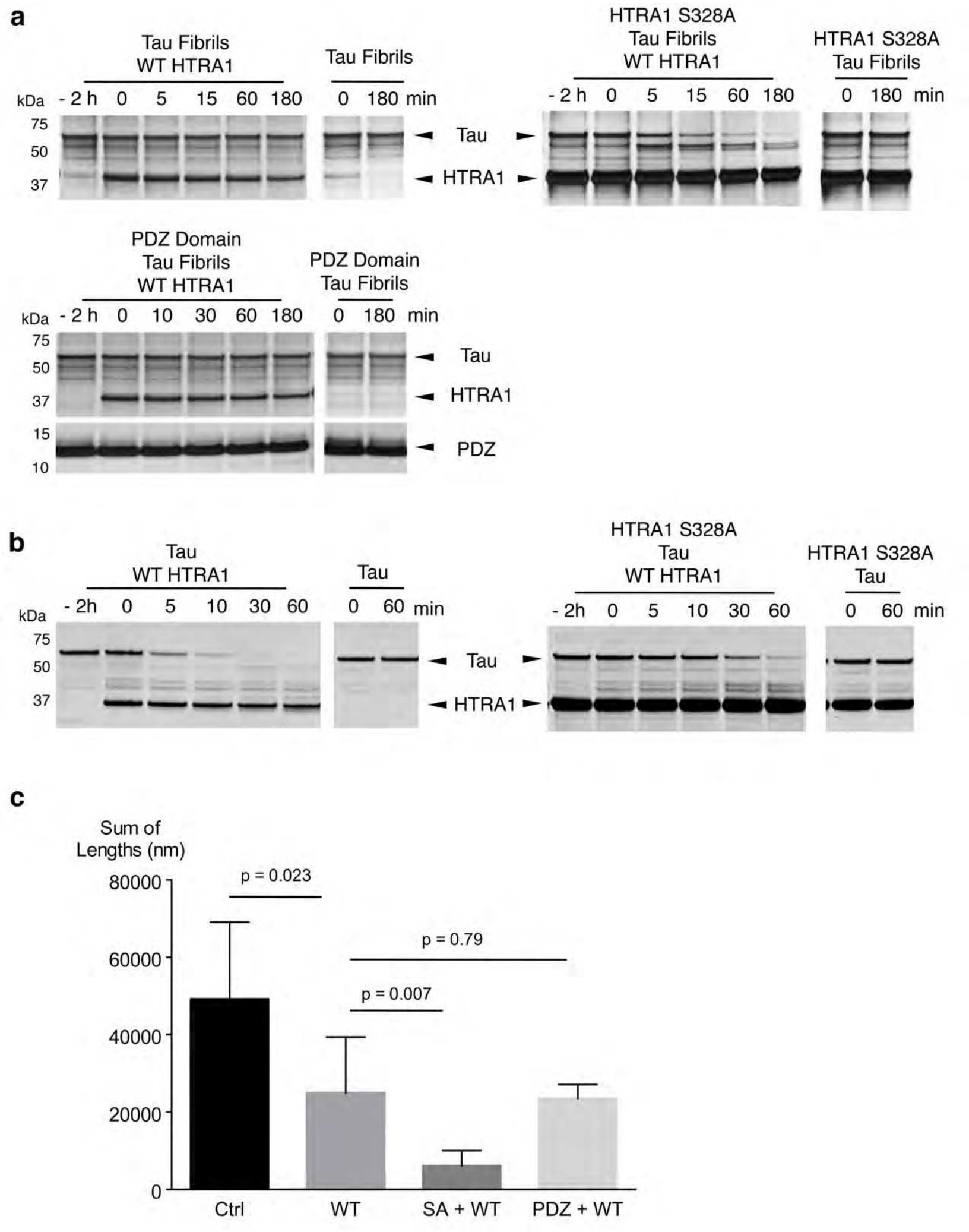
a
Tau Fibrils
WT HTRA1
Tau Fibrils
HTRA1 S328A
Tau Fibrils
WT HTRA1
HTRA1 S328A
Tau Fibrils
kDa
- 2 h 0 5 15 60 180
0 180 min
- 2 h 0 5 15 60 180
0 180 min
75
50
37
Tau
HTRA1
PDZ Domain
Tau Fibrils
WT HTRA1
PDZ Domain
Tau Fibrils
kDa
- 2 h 0 10 30 60 180
0 180 min
75
50
37
15
10
Tau
HTRA1
PDZ
b
Tau
WT HTRA1
Tau
HTRA1 S328A
Tau
WT HTRA1
HTRA1 S328A
Tau
kDa
- 2h 0 5 10 30 60
0 60 min
- 2h 0 5 10 30 60
0 60 min
75
50
37
Tau
HTRA1
c
Sum of
Lengths (nm)
80000
60000
40000
20000
0
p = 0.023
p = 0.79
p = 0.007
Ctrl
WT
SA + WT
PDZ + WT

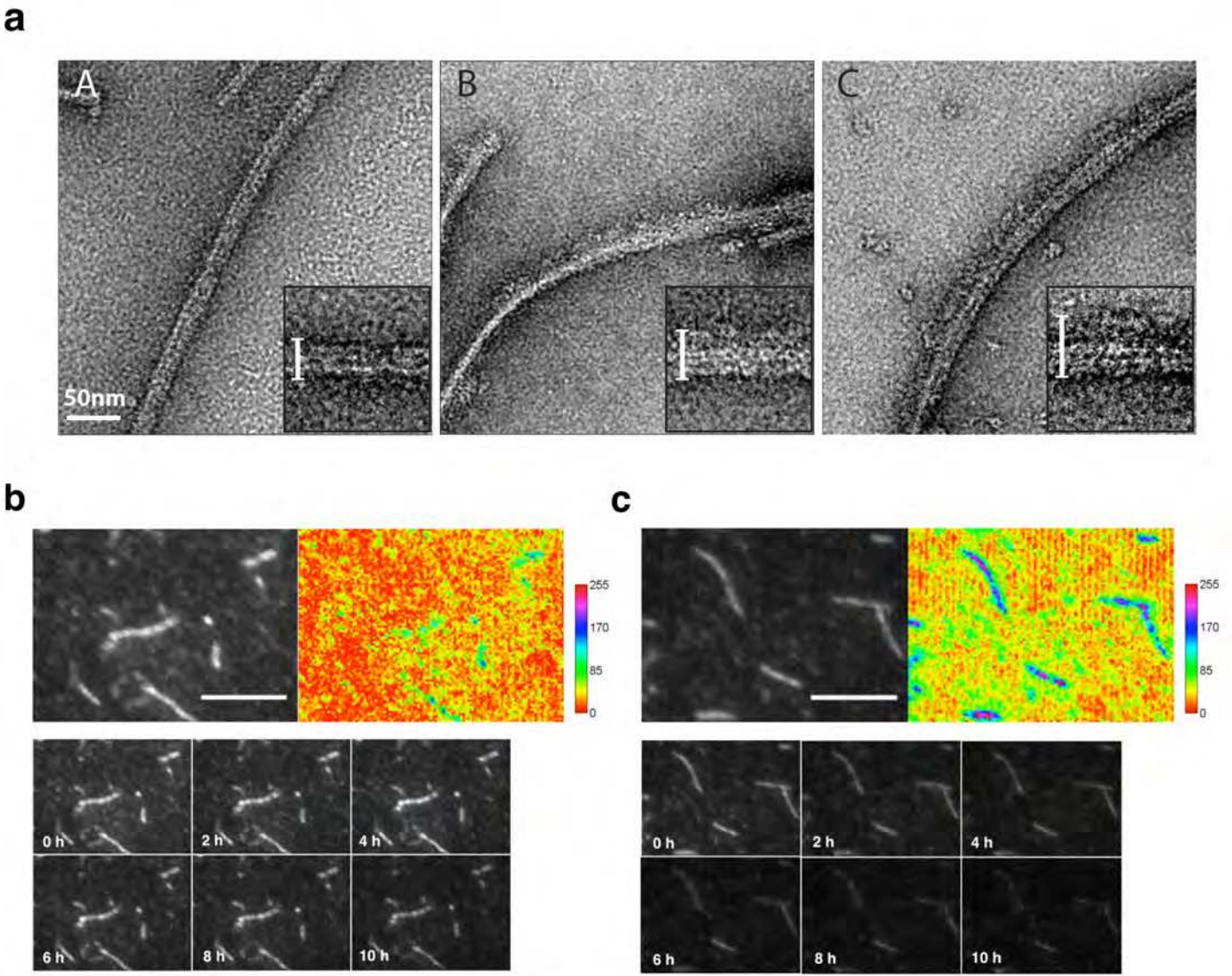
a
A
B
C
50nm
b
255
170
85
0
0 h
2 h
4 h
6 h
8 h
10 h
c
255
170
85
0
0 h
2 h
4 h
6 h
8 h
10 h

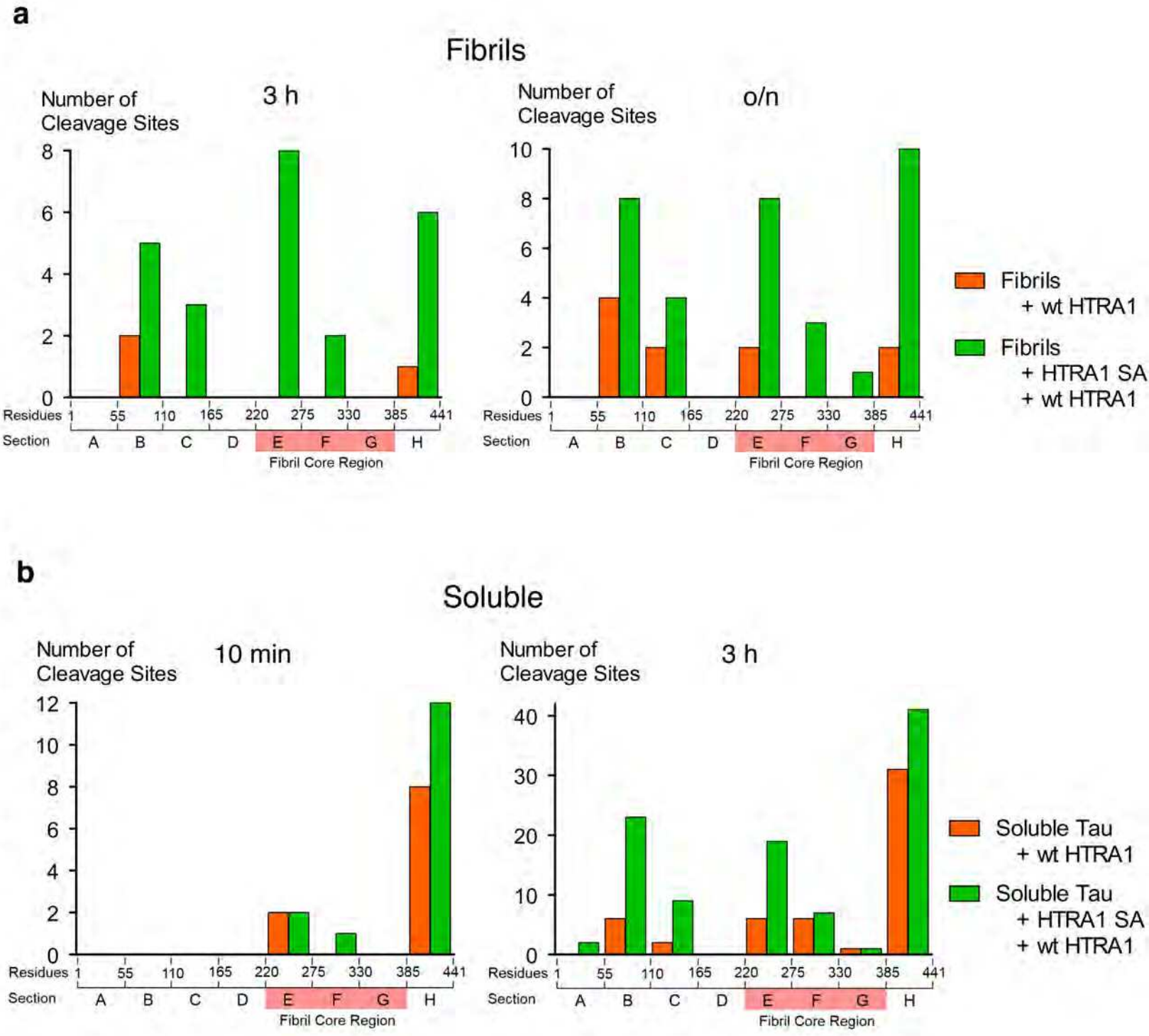
a
Fibrils
3 h
Number of Cleavage Sites
0
2
4
6
8
Residues 1 55 110 165 220 275 330 385 441
Section A B C D E F G H
Fibril Core Region
o/n
Number of Cleavage Sites
0
2
4
6
8
10
Residues 1 55 110 165 220 275 330 385 441
Section A B C D E F G H
Fibril Core Region
Fibrils + wt HTRA1
Fibrils + HTRA1 SA + wt HTRA1
b
Soluble
10 min
Number of Cleavage Sites
0
2
4
6
8
10
12
Residues 1 55 110 165 220 275 330 385 441
Section A B C D E F G H
Fibril Core Region
3 h
Number of Cleavage Sites
0
10
20
30
40
Residues 1 55 110 165 220 275 330 385 441
Section A B C D E F G H
Fibril Core Region
Soluble Tau + wt HTRA1
Soluble Tau + HTRA1 SA + wt HTRA1

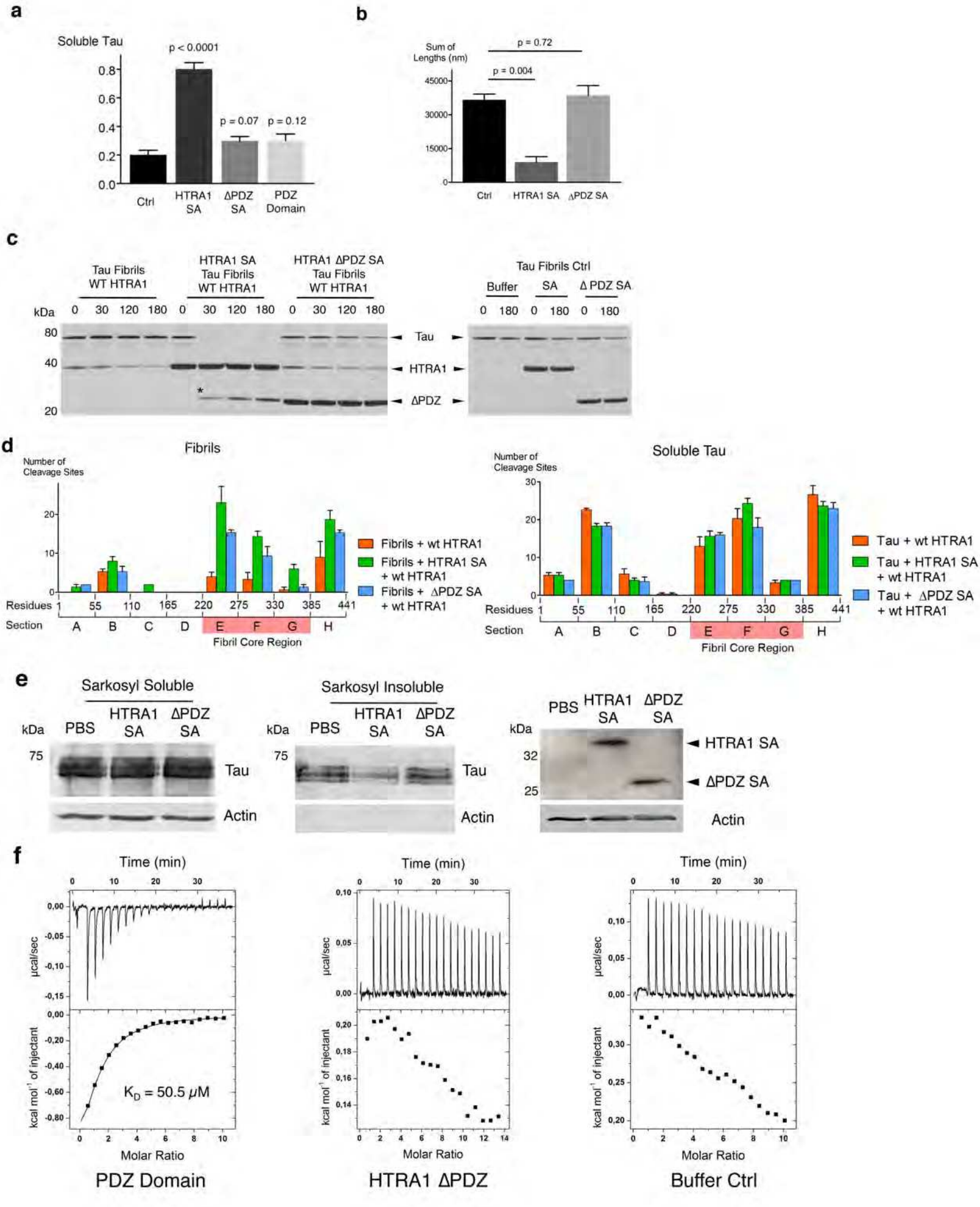
a
Soluble Tau
p < 0.0001
p = 0.07
p = 0.12
Ctrl
HTRA1 SA
ΔPDZ SA
PDZ Domain
b
Sum of Lengths (nm)
p = 0.72
p = 0.004
Ctrl
HTRA1 SA
ΔPDZ SA
c
Tau Fibrils WT HTRA1
HTRA1 SA Tau Fibrils WT HTRA1
HTRA1 ΔPDZ SA Tau Fibrils WT HTRA1
Tau Fibrils Ctrl
Buffer
SA
Δ PDZ SA
kDa
Tau
HTRA1
ΔPDZ
d
Fibrils
Soluble Tau
Number of Cleavage Sites
Residues
Section
Fibril Core Region
Fibrils + wt HTRA1
Fibrils + HTRA1 SA + wt HTRA1
Fibrils + ΔPDZ SA + wt HTRA1
Tau + wt HTRA1
Tau + HTRA1 SA + wt HTRA1
Tau + ΔPDZ SA + wt HTRA1
e
Sarkosyl Soluble
Sarkosyl Insoluble
PBS
HTRA1 SA
ΔPDZ SA
Tau
Actin
f
Time (min)
µcal/sec
kcal mol⁻¹ of injectant
Molar Ratio
K_D = 50.5 µM
PDZ Domain
HTRA1 ΔPDZ
Buffer Ctrl

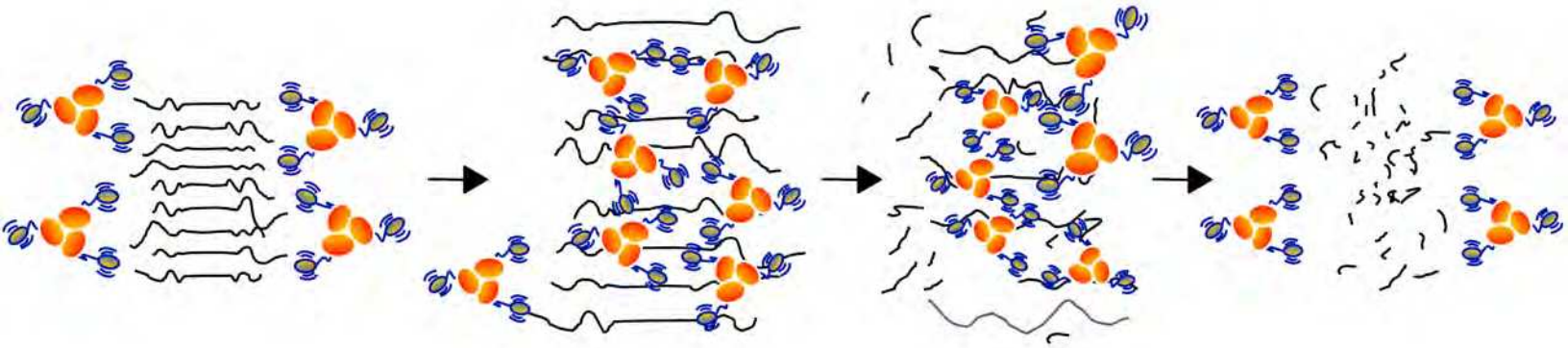

Supplementary Information

Determinants of amyloid fibril degradation by the PDZ protease HTRA1

Simon Pöpsel[1], Andreas Sprengel[1], Barbara Sacca[1], Farnusch Kaschani[1], Markus Kaiser[1], Tim Clausen[2] and Michael Ehrmann[1,3] *

[1] *Centre for Medical Biotechnology, Faculty of Biology, University Duisburg-Essen, Universitaetsstrasse, 45141 Essen, Germany*

[2] *Research Institute of Molecular Pathology – IMP, Dr. Bohrgasse 7, A-1030 Vienna, Austria*

[3] *School of Biosciences, Cardiff University, Cardiff CF10 3US, UK*

[*] **Corresponding author:**

Email: michael.ehrmann@uni-due.de, Phone: +49-201-183 2949

Running title: Proteolysis of amyloid fibrils by HTRA1

Supplementary Results

Supplementary Table 1

Fibrils	A	B	C	D	E	F	G	H
wt HTRA1 + HTRA1 S328A	n/a	0.139 n.s.	n/a	n/a	0.048 *	0.016 *	0.028 *	0.13 n.s.
wt HTRA1 + HTRA1 ΔPDZ S328A	n/a	1 n.s.	n/a	n/a	0.003 **	0.138 n.s.	0.519 n.s.	0.26 n.s.

Soluble Tau	A	B	C	D	E	F	G	H
wt HTRA1 + HTRA1 S328A	1 n.s.	0.028 *	0.37 n.s.	1 n.s.	0.42 n.s.	0.31 n.s.	n/a	0.37 n.s.
wt HTRA1 + HTRA1 ΔPDZ S328A	1 n.s.	0.044 *	0.35 n.s.	n/a	0.37 n.s.	0.57 n.s.	n/a	0.37 n.s.

Statistical analysis of the number of cleavage sites in tau fibrils or soluble tau. p-values of wt HTRA1 vs. (wt HTRA1 + HTRA1 S328A) and of wt HTRA1vs. (wt HTRA1 + HTRA1 ΔPDZ S328A). The number of cleavage sites in fibrils or soluble tau by wt HTRA1 were compared with the respective numbers after incubation with HTRA1 S328A and HTRA1 ΔPDZ S328A as shown in Fig. 6d, using a two-tailed t-test for unpaired samples with Welch's correction for unequal variances in GraphPad Prism. n.s. = not significant, * = $p < 0.05$, ** = $p < 0.01$, n/a = not applicable. n = three independent experiments.

Supplementary Figures

Supplementary Figure 1
(a), (b) Quantification of fibril disintegration by HTRA1 S328A. (a) Quantification of band intensities and analysis of the ratio of soluble versus total tau (n=4). p-values are according to a two-sided t-test for unpaired datasets with Welch's correction for unequal variances. (b) Titration of HTRA1 S328A in sedimentation assay. Tau fibrils were incubated with HTRA1 at the indicated molar ratios, followed by ultracentrifugation. Solubilization of fibrils was quantified as the ratio of soluble versus total tau. Data points represent the mean of 4-8 independent assays, error bars are SEM. *(c), (d)Sedimentation assay of MTBD tau fibrils*. (c) 6.7 μM MTBD tau fibrils were incubated with a 3 fold molar excess of proteolytically inactive HTRA1 S328A (HTRA1 SA) or Aldolase at 37°C for 16 h followed by ultracentrifugation. Subsequently, samples before centrifugation (T, total), of pellet (P) and supernatant (S) fractions were subjected to SDS-PAGE followed by immunoblotting against the repeat region of tau. The samples were subjected to SDS-PAGE followed by Coomassie staining to detect HTRA1 and control protein in the presence of MTBD fibrils (middle panel) or after incubation without tau as a control (bottom panel). (d) Quantification of MTBD solubilization based on the band intensities of soluble versus total tau samples in the blots shown in (c). The indicated p-values were computed with a two-sided t-test for unpaired samples with Welch's correction for unequal variances in GraphPad Prism.

Supplementary Figure 2
(a), (b) Quantification of AFM analysis of fibril disintegration. Quantification of fibril abundance based on image analysis of 4 random 3 x 3 μm views per sample. Fibrils were treated with HTRA1 S328A or the isolated PDZ domain of HTRA1 as shown in Fig. 1, b and c. Columns represent the mean of total fibril lengths per view. Error bars are SEM. p-values indicate statistical significance according to a two-sided t-test for unpaired datasets with Welch's correction. For each condition > 100 individual fibrils were included into statistical analyses. (c) *Distribution of fibril size after disintegration by HTRA1 S328A*. The lengths of individual tau fibrils were measured in at least 3-4 individual regions of samples as described in Fig. 1. The distribution of fibril size was assessed by means of a frequency distribution using a bin width, i.e. the length intervals to be analyzed, of 50 nm. The relative frequency of fibrils in the respective length intervals was plotted. The displayed lengths were limited to < 1200 nm because only a minor number of fibrils exceeded this value.

Supplementary Figure 3
Internalization of recombinant HTRA1 by cultured 293T HEK cells. Cells were incubated for 6 h with culture medium conditioned with increasing concentrations of HTRA1 (a) or with a fixed amount of HTRA1 (150 μg/ml = 4.1 μM) for the incubation times indicated (b). Lysates of trypsinized cells were subjected to SDS-PAGE and immunoblotting using antibodies against HTRA1 and Actin (loading control). As controls, cells were treated with PBS or 4.1 μM HTRA1 followed by incubation at 4°C for 6 h. (c-d) Uptake of fluorescently labeled HTRA1 S328A by 293T HEK cells followed by confocal microscopy. Cells were treated with 50 μg/ml (= 1.35 μM) HTRA1 or PBS (control) for 16 h, followed by methanol fixation and immunostaining against HTRA1 (c) or the HA tag (d) of transiently overexpressed tau as indicated. DAPI was used as nuclear counterstain. The images show the dispersed cytoplasmic or vesicular localization of internalized HTRA1 S328A (labeled with AF 568) (c) and positive immunostaining of HTRA1 and colocalization with its native cytoplasmic substrate tau (αHA antibody) (d). (e) Secondary antibody (2°AB) control of internalized, fluorescently labeled HTRA1. 293T HEK cells were treated with HTRA1

conditioned medium for 20 h, followed by fixation and staining as described above except for the primary antibody against HTRA1 being omitted in order to exclude unspecific staining of labeled HTRA1 or the AlexaFluor 568 dye by the secondary antibody. Scale bars, 25 μm. The data are representative of at least 2 biological replicates.

Supplementary Figure 4

Cell based assay of fibril degradation by HTRA1. (a) Analysis of the amount of sarkosyl insoluble tau in the HTRA1 S328A treated cells relative to the PBS controls (n=4) Error bar is SEM. p-values were calculated with GraphPad Prism using a to a two-tailed, paired t-test. (b) 293T HEK cells were treated as described in Fig. 2. After seeding, cells were treated with culture medium conditioned with proteolytically active HTRA1 (wt) (4.1 μM) or PBS for 20 h followed by lysis, sarkosyl extraction and immunoblotting of sarkosyl soluble (left panel) and insoluble (pellet, right panel) fractions against tau, and immunoblotting of the sarkosyl soluble fractions against HTRA1 to detect the uptake of recombinant wt HTRA1 (lower left panel). Lower right panel: Analysis of the amount of Sarkosyl insoluble tau in the wt HTRA1 treated cells relative to the PBS controls. Data from 3 independent experiments, error bar represents the SEM. Decrease is highly significant according to a two-tailed, paired t-test, computed with GraphPad Prism.

Supplementary Figure 5

(a) Tau fibrils (left) or soluble tau (right) were proteolyzed by wt HTRA1 present in the concentration corresponding to HTRA1 S328A in Fig. 3 (a) and (b). Samples were treated as described in Fig. 3 and subjected to SDS-PAGE and silver staining (n=3). (b) Representative images of AFM analysis of Tau proteolysis by wt HTRA1 following incubation with buffer (top right), HTRA1 S328A (bottom left) or the isolated PDZ domain of HTRA1 (bottom right) as compared to the control incubated without wt HTRA1 (top left). (c) Distribution of fibril lengths after disintegration and proteolysis by HTRA1. Changes in the abundance of fibrils depending on their lengths were analyzed as described for the AFM data of disintegrated fibrils (Fig. 1b,c and Supplementary Fig. 2). The distribution of fibril lengths is shown as the relative frequency to assess changes in the lengths of fibrils.

Supplementary Figure 6

Proteolysis of labeled tau fibrils observed by TIRFM. (a) Decrease in fluorescence was analyzed with respect to the relative position along single fibrils to quantify the distribution of the total fluorescence decrease. Error bars are SEM. Scale bars, 5 μm. The data is representative of 2 biological and at least 4 technical replicates. (b) Decrease in the fluorescence intensity of individual fibrils in the buffer control (black circles) and in the presence of HTRA1 (green squares) as measured by TIRF microscopy. The values shown are the means of intensities relative to the fluorescence measured at t_{0h} of 300-400 ROIs representing single or overlapping fibrils for each time point and sample as described. The data used originated from a single dataset. The error bars indicate the standard deviation. The total decrease in fluorescence was 29% in the buffer control versus 68% in the presence of wt HTRA1. (c) Representative endpoint images after 14 h of incubation of tau fibrils with buffer (top row) or 1 μM wt HTRA1 (bottom row) to illustrate the decreased fluorescence caused by the proteolysis of fibrils by HTRA1 irrespective of photobleaching. The images are shown with a spectrum LUT (left) for the visualization of the pixel intensities and as greyscale images for overview (middle). In the right panels, the regions highlighted by white boxes are zoomed in. Scale bars, 25 μm and 10 μm for overview and zoomed-in images, respectively. Representative images of 3 independent experiments are shown.

Supplementary Figure 7

K_D of tau Peptides Determined by ITC. (Top panel) Representative ITC raw data and the binding isotherm based on the integrated heat changes are shown in the top and bottom part of the figure, respectively. The exemplary data represent the measurement of the peptide KTDHGAEIV corresponding to aa 385-393 of 4R tau. (Bottom panel) List of peptide sequences, their position within the aa sequence of tau and the K_Ds measured by ITC. Numbers correspond to μM values. For the ITC measurements, 2 μl of a 2 mM solution of the respective peptides were injected into the sample cell containing 20 μM HTRA1. The area under each peak was integrated and plotted against the molar ratio peptide/HTRA1 in the sample cell. The black line represents the fit to a binding isotherm according to the one set of sites fitting mode. n.d. = not detected (no binding).

Supplementary Figure 8

Representative images of fibrils disintegration by HTRA1 S328A versus HTRA1 ΔPDZ S328A as analyzed by sedimentation (a) or AFM (b) assays as in Fig. 1. (c) Sedimentation Assay with MTBD Aggregates and HTRA1 ΔPDZ S328A. Sedimentation assays were performed as in Supplementary Fig. 1, except that in addition to buffer control and HTRA1 S328A, HTRA1 ΔPDZ S328A and the isolated, recombinant PDZ domain were used. Top panel represents anti-tau immunoblots to visualize the MTBD of tau in the total (T), pellet (P) and supernatant (S) fractions. The middle and bottom panels show Coomassie stained gels of the reaction with and without MTBD tau to illustrate the solubility of the proteins added to tau. (d) Quantification of the band intensities of 4 independent experiments with the mean and SEM are shown. The indicated p-values were calculated according to a two-tailed t-test for unpaired datasets with Welch's correction for unequal variances in GraphPad Prism. (e) Analysis of the amount of sarkosyl insoluble tau in HTRA1 S328A and HTRA1 ΔPDZ S328A treated cells relative to the PBS controls (n=4). Error bars are SEM. p values were computed with GraphPad Prism using a two-tailed, paired t-test.

Supplementary Figure 9

Disintegration of $A\beta_{1-42}$ Aggregates by HTRA1 S328A. 50 μM $A\beta_{1-42}$ (Aβ) were incubated with equimolar amounts of HTRA1 S328A or the control protein MDH, followed by ultracentrifugation and the analysis of samples from the disintegration reaction (T, total), the pellet (P) and supernatant (S) by SDS-PAGE and silver staining. The data are representative of 3 independent experiments.

Supplementary videos

Supplementary Video 1 *TIRF microscopy of fibril degradation*. Fluorescently labeled tau fibrils adhering to microscopy slides were incubated with wt HTRA1. Proteolytic degradation of fibrils was followed by recording 120 images over a period of 4 h.

Supplementary Video 2 *TIRF microscopy of tau fibrils*. To detect photobleaching, imaging of tau fibrils was performed in the absence of HTRA1 as described in Supplementary Video 1.

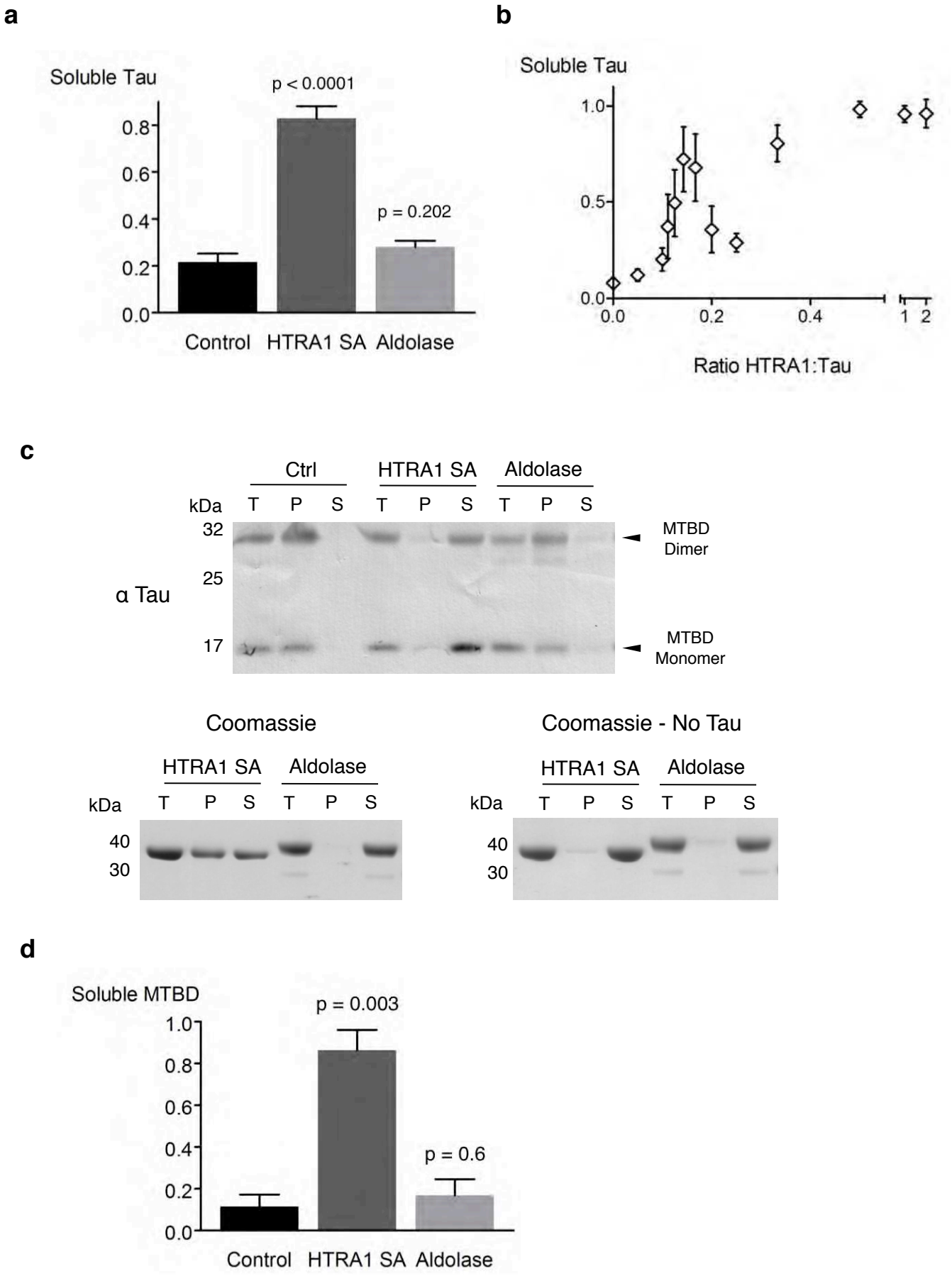

Supplementary Figure 1

Fibril Lengths by Relative Frequency

a

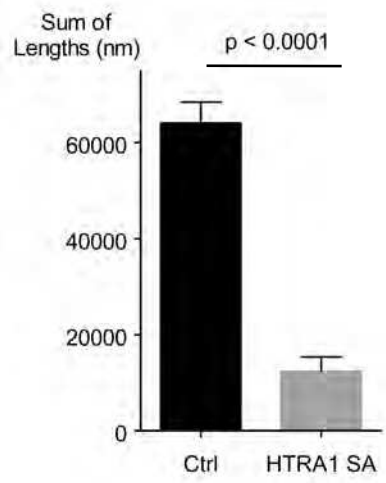

b

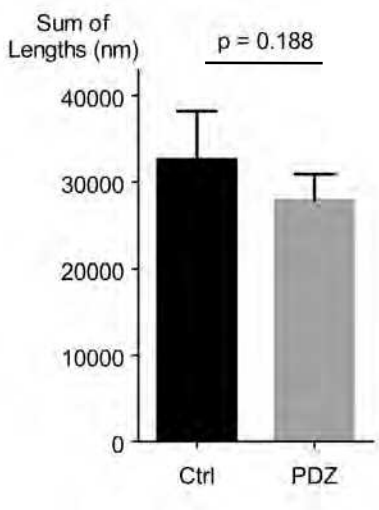

c

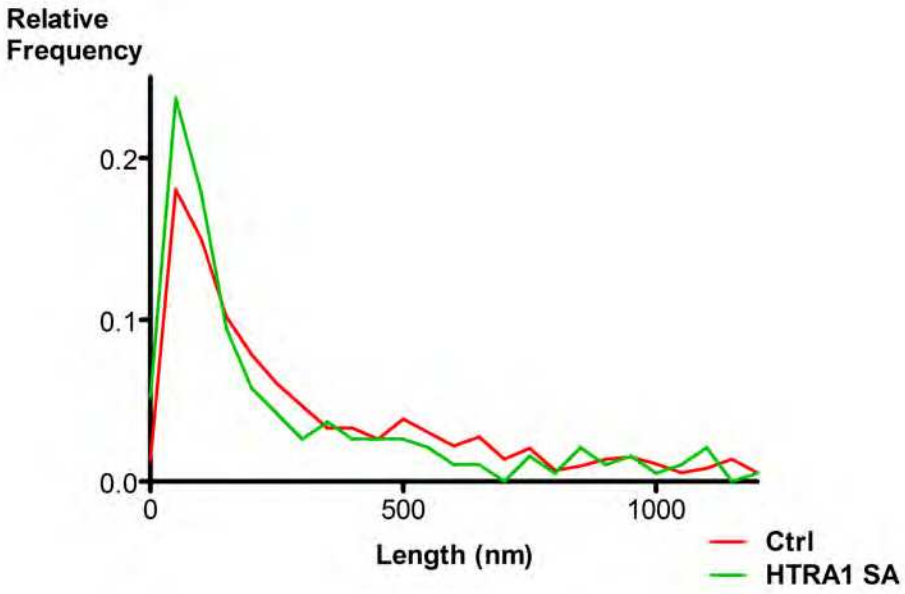

Supplementary Figure 2

a – *Titration of Recombinant HTRA1*

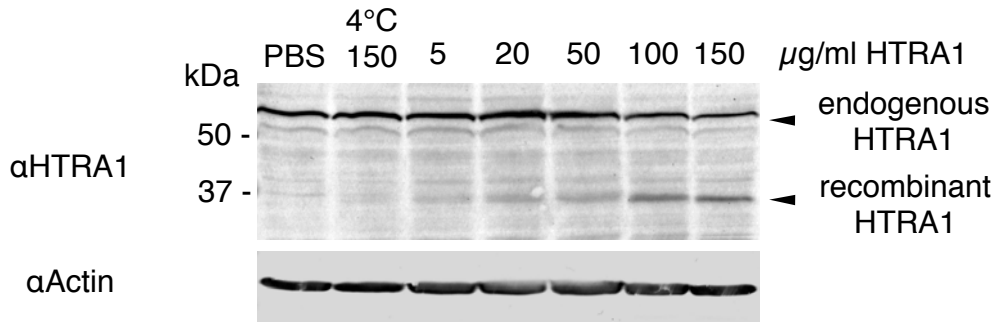

b – *Time-course of Internalization*

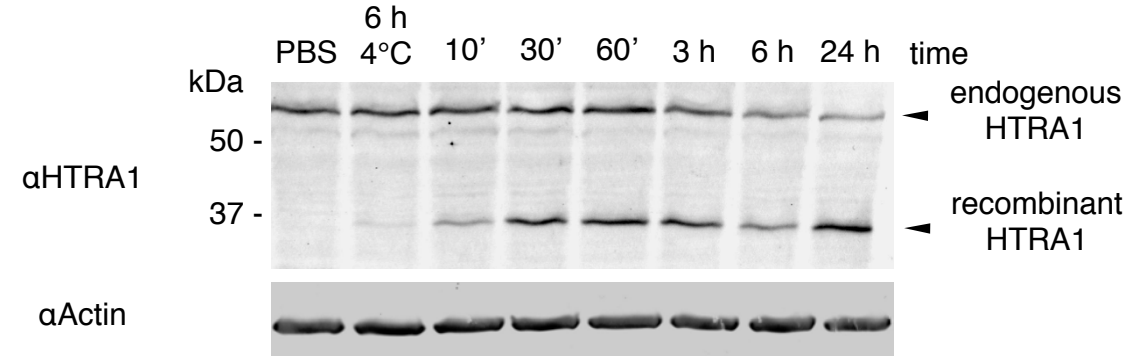

c – *Localization of Internalized Labelled HTRA1 S328A and αHTRA1 immunostaining*

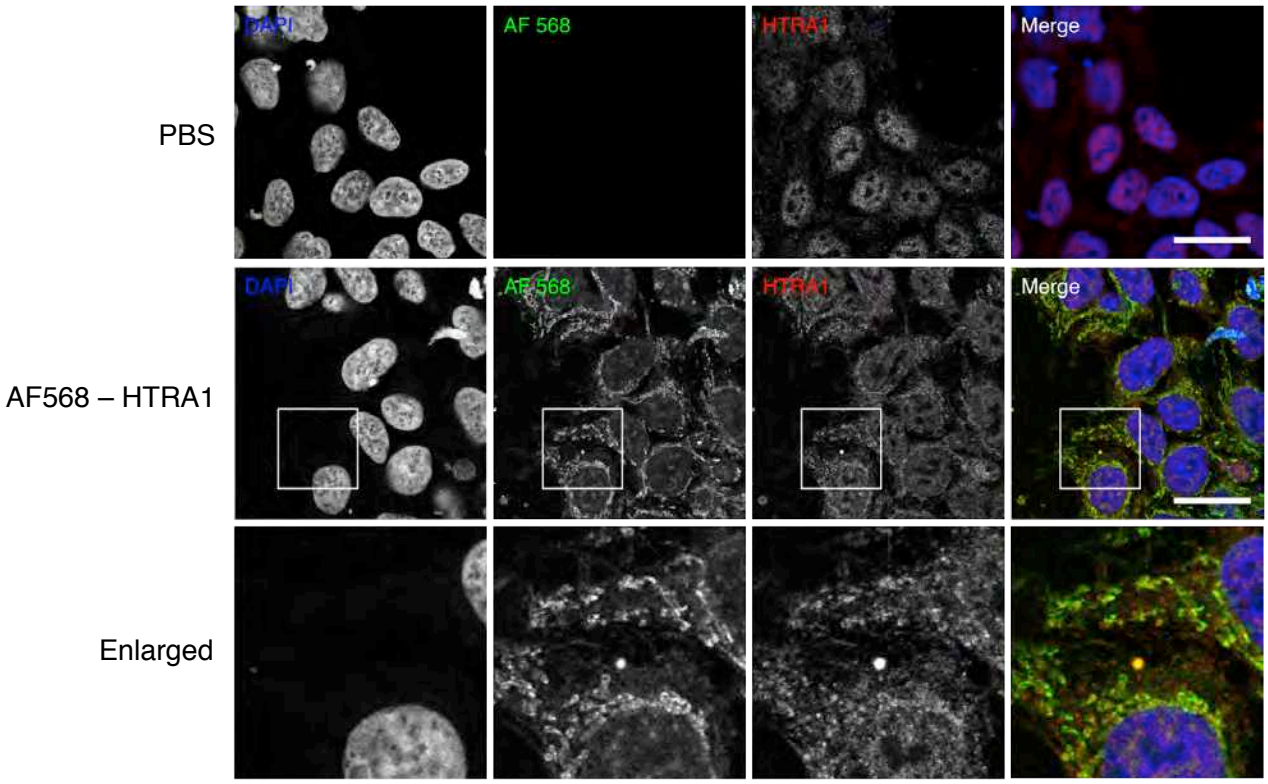

Supplementary Figure 3

d – *Colocalization of Internalized Labelled HTRA1 SA with HA-tagged Tau , αHA Tag Staining*

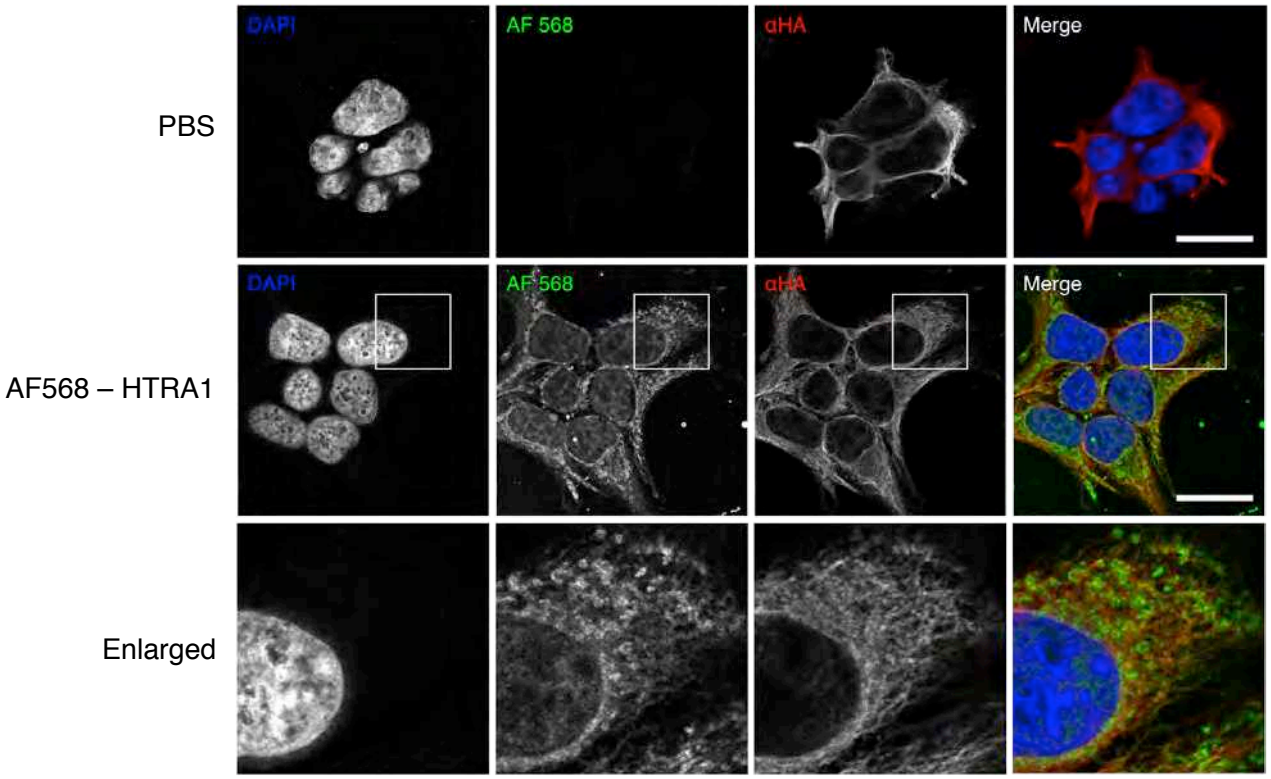

e – *Secondary Antibody Ctrl of Internalized HTRA1*

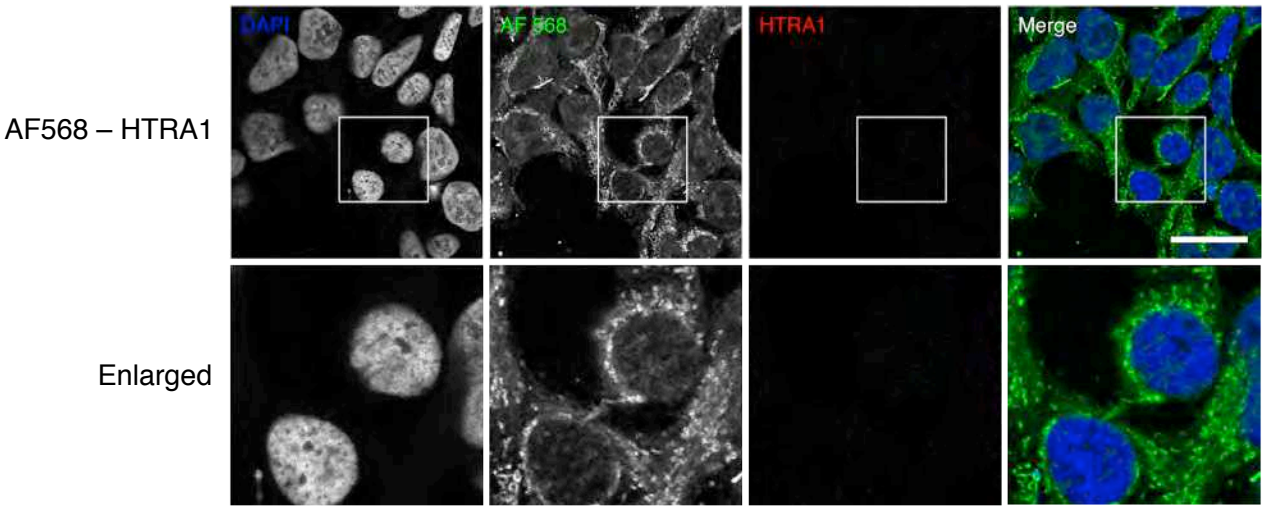

Supplementary Figure 3

a

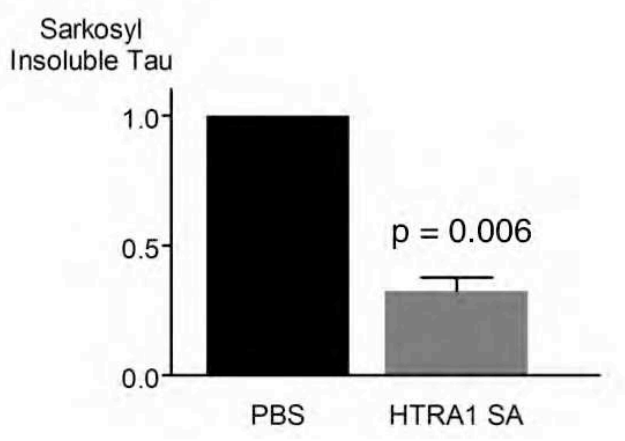

b

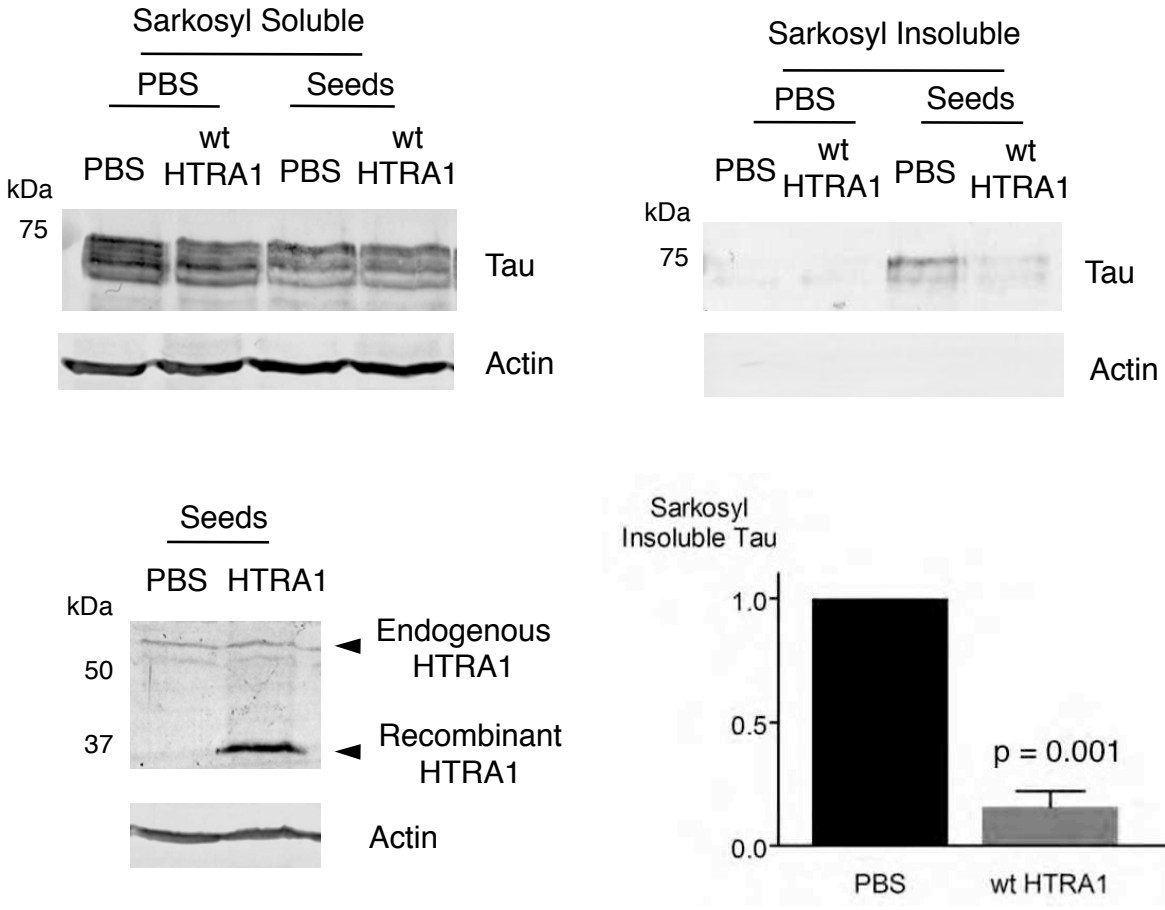

Supplementary Figure 4

Fibril Lengths after Proteolysis by Relative Frequency

a

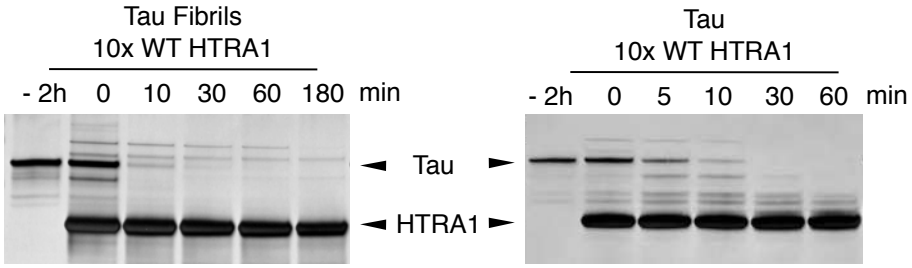

b

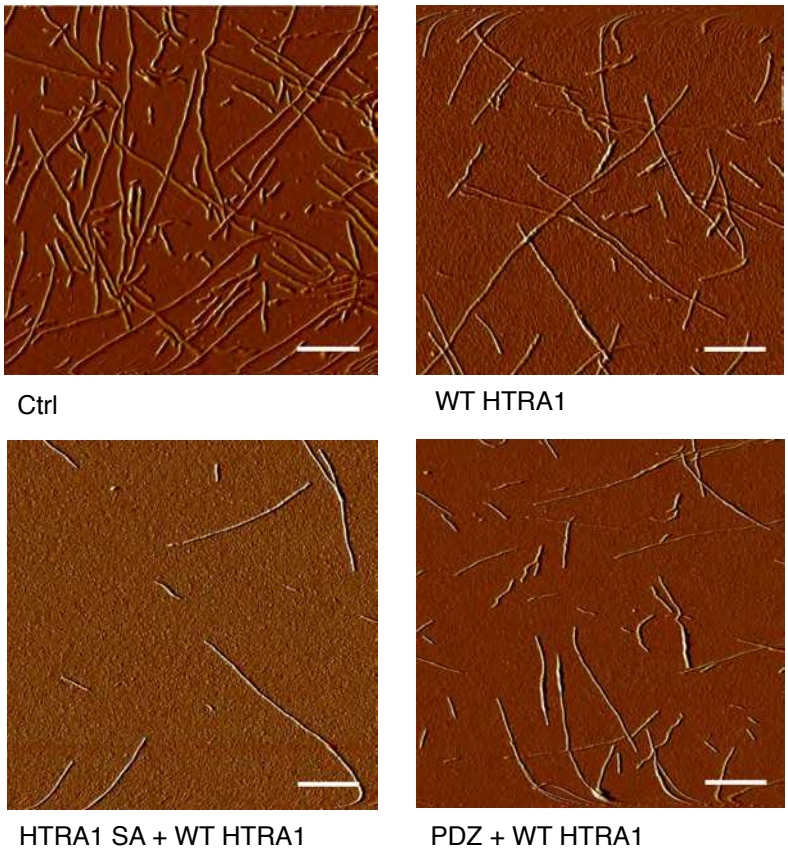

c

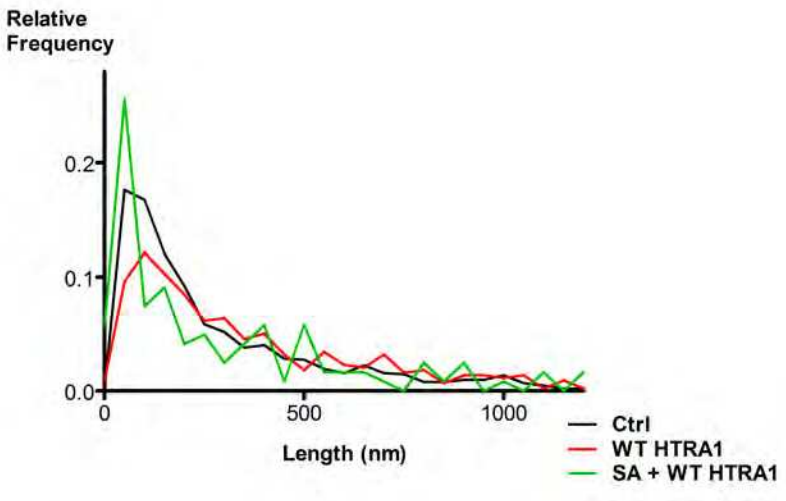

Supplementary Figure 5

a

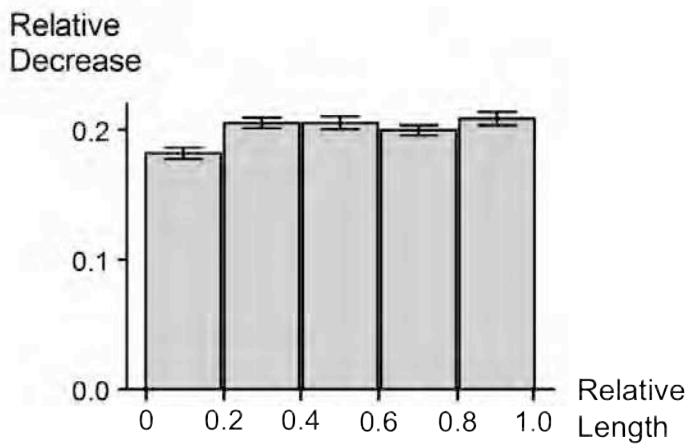

b

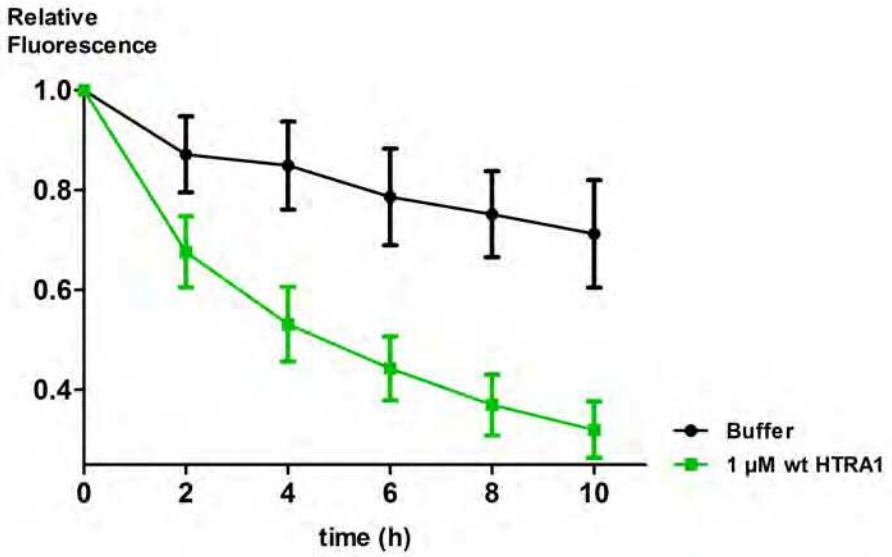

c

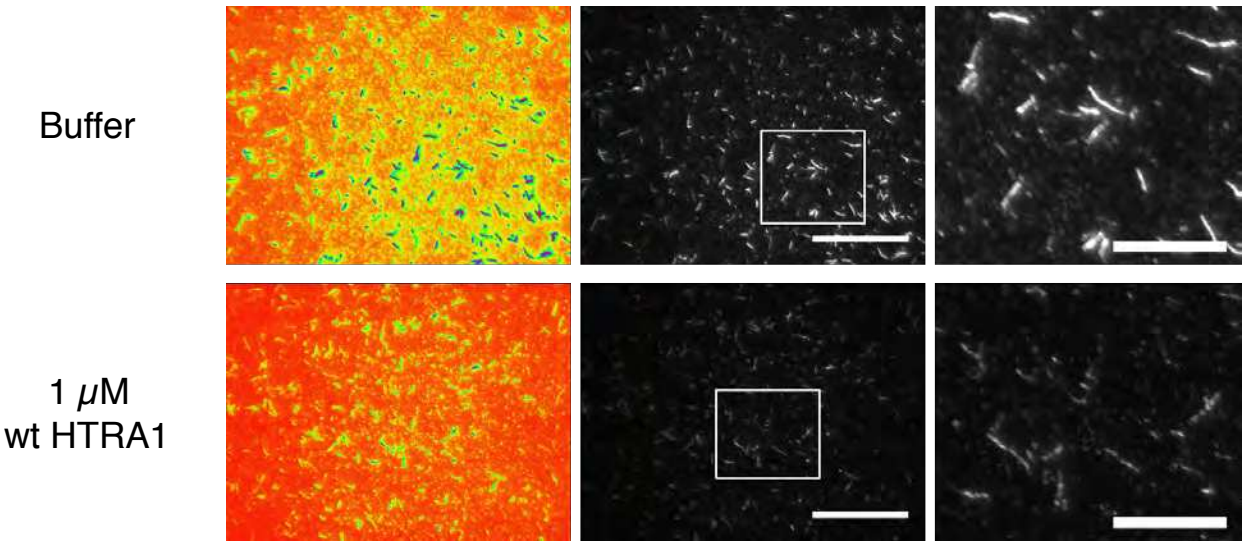

Supplementary Figure 6

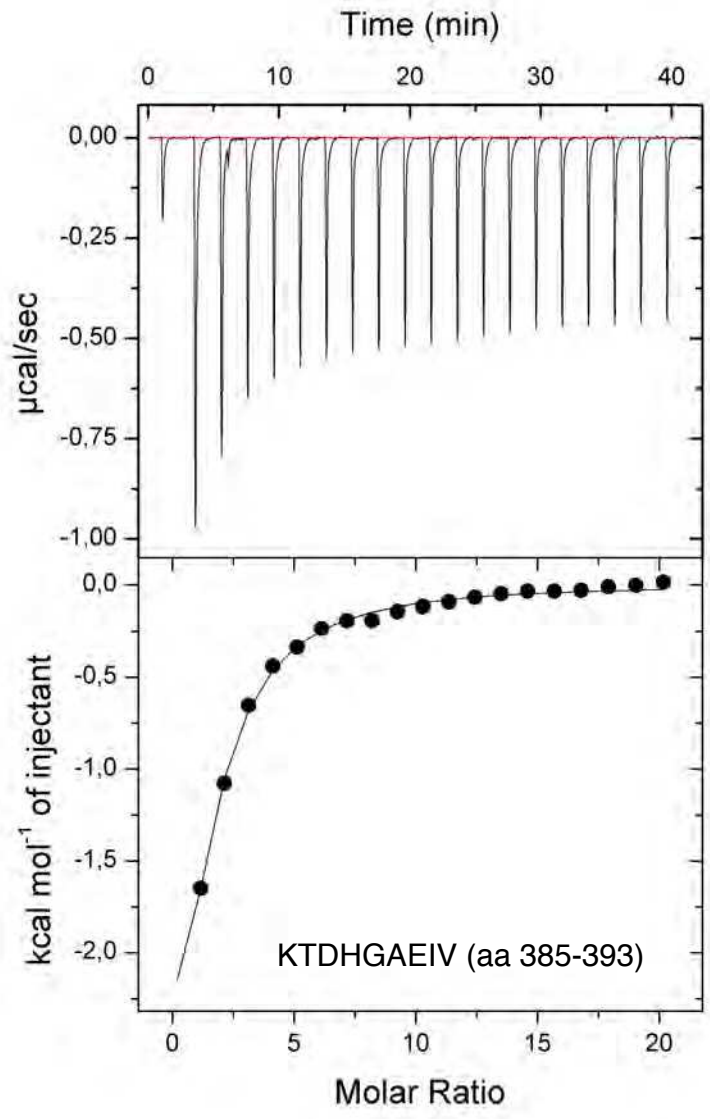

aa in tau	Sequence	K_D
308-319	KHVPGGGSVQIV	25
385-393	KTDHGAEIV	35
385-399	KTDHGAEIVYKSPVV	40
246-256	PVPMPDLKNV	n.d.
401-416	DTSPRHLSNVSSTGSI	n.d.

Supplementary Figure 7

Disintegration Assay with MTBD Aggregates and HTRA1 ΔPDZ S328A

a

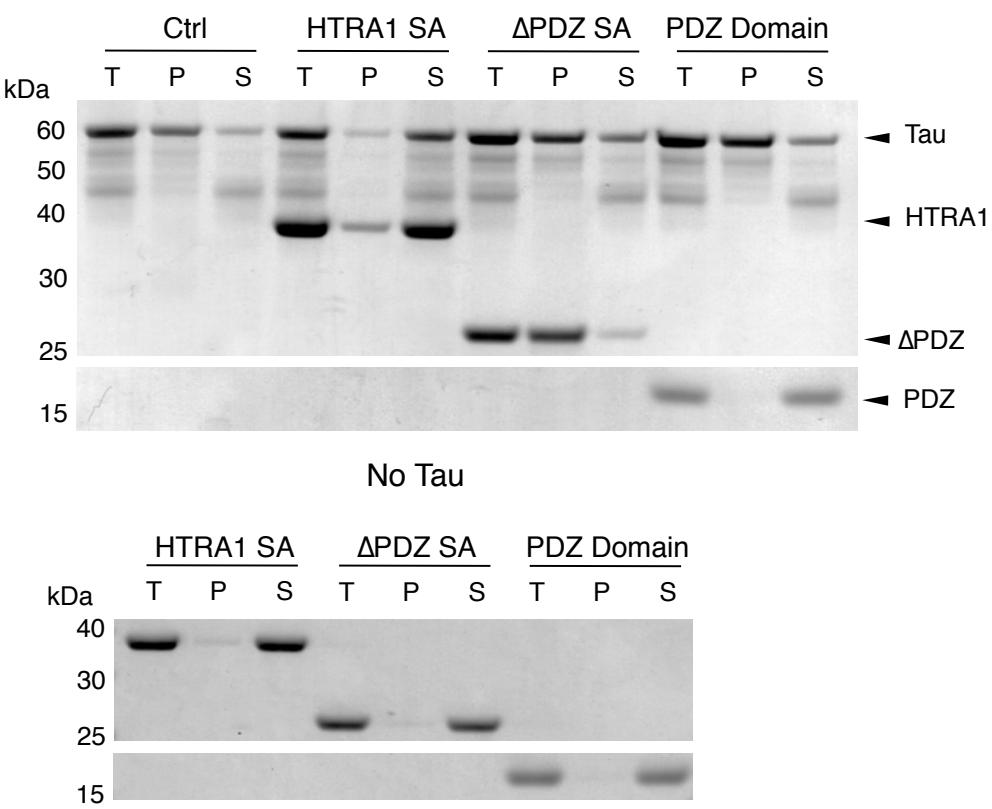

b

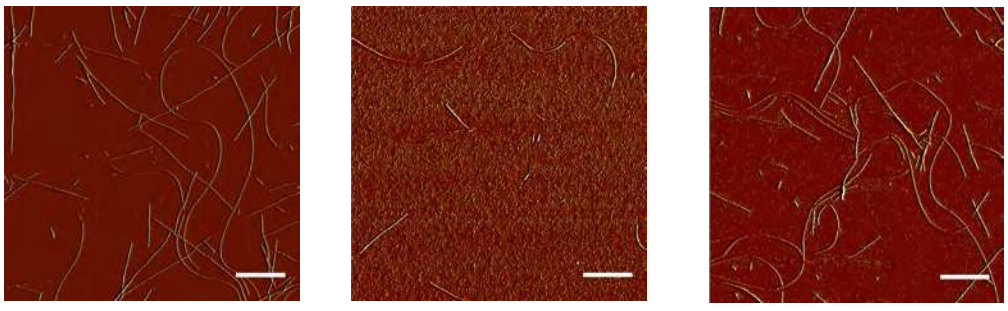

Supplementary Figure 8

Disintegration Assay with MTBD Aggregates and HTRA1 ΔPDZ S328A

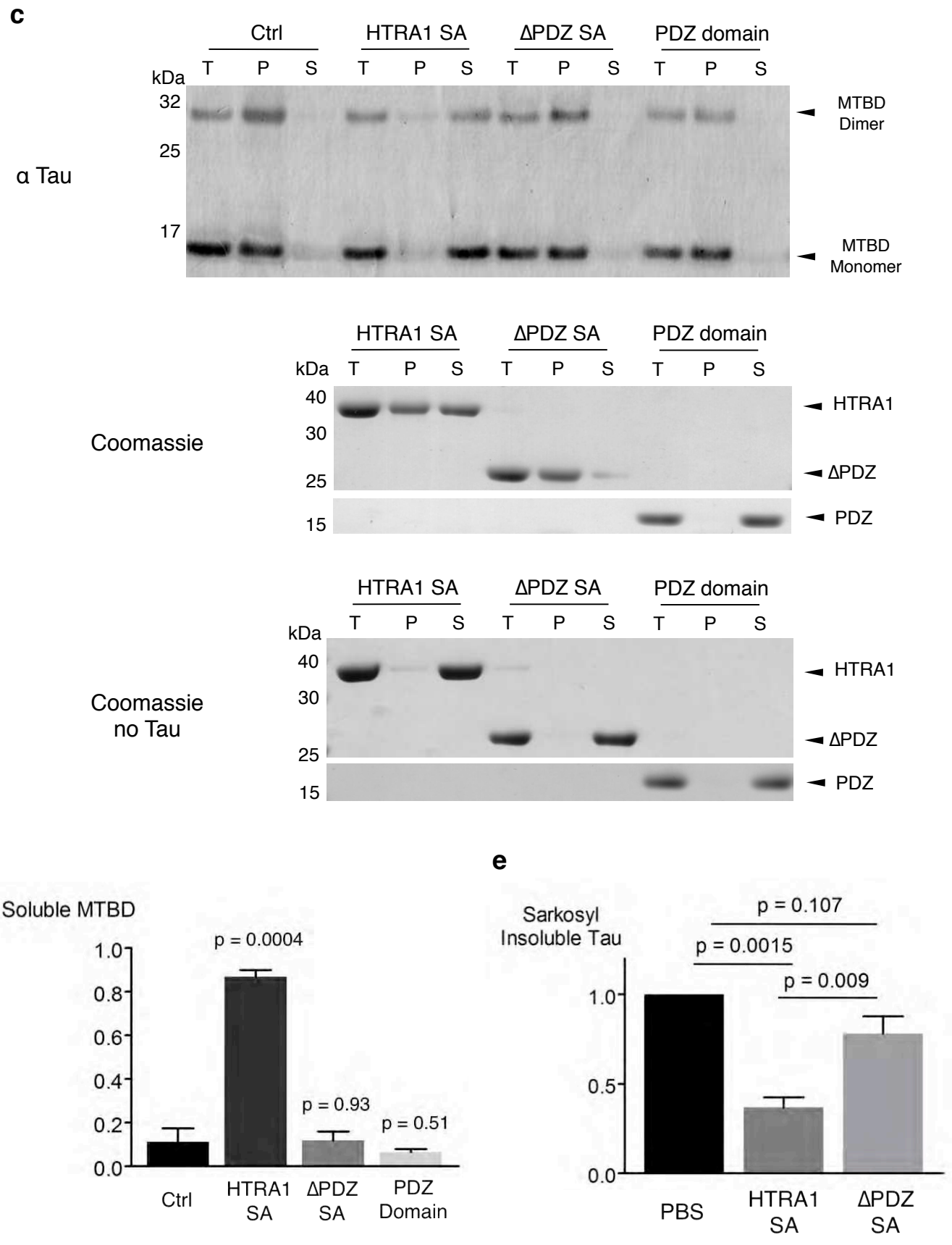

Supplementary Figure 8

Sedimentation Assay of Aβ Aggregates

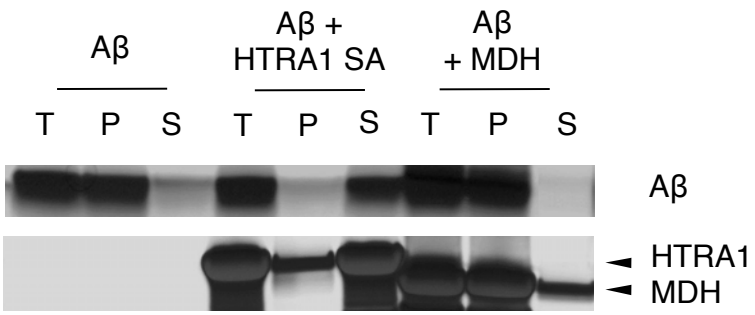

Supplementary Figure 9